

NASA CR-168171



National Aeronautics and  
Space Administration

# NONLINEAR DAMAGE ANALYSIS — POSTULATE AND EVALUATION

March 1983

by

B.N. Leis and T.P. Forte

BATTELLE-COLUMBUS LABORATORIES

(NASA-CR-168171) NONLINEAR DAMAGE ANALYSIS:  
POSTULATE AND EVALUATION Final Report, 30  
Sep. 1981 - 6 Apr. 1983 (Battelle Columbus  
Labs., Ohio.) 101 p HC A06/MF A01 CSCL 20K

N86-26652

Unclas  
G3/39 43429

Prepared for

National Aeronautics and Space Administration

LEWIS RESEARCH CENTER  
Contract NAS3-22825

1 Report No CR 168171	2 Government Accession No	3 Recipient's Catalog No	
4 Title and Subtitle Nonlinear Damage Analysis -- Postulate and Evaluation		5 Report Date April 6, 1983	6 Performing Organization Code
		8 Performing Organization Report No	
7. Author(s) B. N. Leis and T. P. Forte		10 Work Unit No	
9. Performing Organization Name and Address Battelle Columbus Laboratories 505 King Avenue Columbus, Ohio 43201		11 Contract or Grant No. NAS 3-22825	
		13. Type of Report and Period Covered Final 9/30/81-4/6/83	
12 Sponsoring Agency Name and Address NASA Lewis Research Center 21000 Brookpark Road Cleveland, Ohio 44135		14 Sponsoring Agency Code	
15 Supplementary Notes			
16 Abstract <p>The objective of this program was to assess the viability of a damage postulate which asserted that the fatigue resistance curve of a metal is history dependent due to inelastic action. The study focussed on OFE copper because this simple model material accentuated the inelastic action central to the damage postulate. Data relevant to damage evolution and crack initiation were developed via a study of surface topography. The effects of surface layer residual stresses were explored via comparative testing as were the effects in initial prestraining.</p> <p>The results of the study very clearly indicated the deformation history dependence of the fatigue resistance of OFE copper. Furthermore the concept of deformation history dependence was shown to qualitatively explain the fatigue resistance of all histories considered. Likewise quantitative predictions for block cycle histories were found to accurately track the observed results. In this respect the assertion that damage per cycle for a given level of the damage parameter is deformation history dependent appears to physically justified. Also, use of a history dependent nonlinear assessment quantitative predictions of life to form a small crack when damage was linearly accumulated.</p>			
17. Key Words (Suggested by Author(s)) Fatigue Crack initiation Life Prediction Damage Assessment Damage Accumulation OFE Copper		18. Distribution Statement	
19. Security Classif (of this report) Unclassified	20 Security Classif. (of this page) Unclassified	21 No of Pages	22 Price*

\* For sale by the National Technical Information Service Springfield Virginia 22161



## TABLE OF CONTENTS

	<u>Page</u>
FORWARD . . . . .	1
INTRODUCTION . . . . .	1
APPROACH AND SCOPE . . . . .	3
DAMAGE ANALYSIS . . . . .	6
Concepts Involved in Damage Analysis . . . . .	6
Damage . . . . .	6
Damage Parameters . . . . .	6
Similitude . . . . .	8
Operational Definition of Nucleation . . . . .	10
Phenomenology Relevant to Damage Analysis . . . . .	12
Assumptions . . . . .	13
Important Questions . . . . .	14
THE DAMAGE POSTULATE . . . . .	15
EXPERIMENTAL ASPECTS . . . . .	17
Test Matrix . . . . .	17
Data Requirements . . . . .	17
Approach to Meet Objectives . . . . .	18
Test Plan . . . . .	20
Experimental Details . . . . .	20
Material and Specimen . . . . .	20
Apparatus and Procedure . . . . .	24
RESULTS AND DISCUSSION . . . . .	30
Material Characterization . . . . .	30
Damage Evolution and Crack Detection . . . . .	33
Stress Response . . . . .	33
Ultrasonics . . . . .	37
Surface Topography . . . . .	38
Microhardness . . . . .	52
Cyclic Deformation and Fatigue Behavior . . . . .	54

TABLE OF CONTENTS  
(Continued)

	<u>Page</u>
Surface Topography . . . . .	58
Surface Stress States . . . . .	59
Measures of Damage . . . . .	60
History Dependence of the Fatigue Resistance . . . . .	63
EXAMINATION OF THE DAMAGE POSTULATE . . . . .	65
History Dependence in a Strain Based Framework . . . . .	65
History Dependence in the Absence of Transient Effects . . . . .	70
Damage Assessment and Accumulation Predictions for Block Cycling . . . . .	78
Commentary . . . . .	83
SUMMARY . . . . .	84
CONCLUSIONS . . . . .	85
REFERENCES . . . . .	87

LIST OF TABLES

Table 1. Test Plan . . . . .	21
Table 2 Area and Crack Depth as a Function of Load Drop . . . . .	36
Table 3. Surface Topography Study . . . . .	40
Table 4. Change in Bulk Microhardness in OFE Copper Under CA Cycling to Initiation . . . . .	53
Table 5. Fatigue Resistance Data Developed Following the Test Plan of Table 1 . . . . .	56
Table 6. Parameters Related to the Fatigue Resistance Data Presented in Table 5 . . . . .	57

LIST OF FIGURES

Figure 1. Typical Application of a Damage Parameter Used to Consolidate Multiaxial Fatigue Resistance of 1015 Mild Steel - $\Delta\bar{\epsilon}$ and $\Delta\bar{\epsilon}^t$ Are Equivalent Uniaxial Measures of Stress Range and Total Strain Range . . . . .	9
---	---

LIST OF FIGURES  
(Continued)

	<u>Page</u>
Figure 2. Schematic Illustrating the Back Extrapolation Procedure to Define Nucleation (OFE Copper, $N_f = 853$ Cycles) . . . . .	11
Figure 3. Essential Features of the Damage Analysis Postulate . . . . .	16
Figure 4. Axial Fatigue Test Specimen . . . . .	23
Figure 5. Evidence of $Cu_2O$ Formation . . . . .	26
Figure 6. Evidence of $Cu_2O$ and Its Apparent Influence on Initiation . . . . .	27
Figure 7. Overview of Test Cell and Gripping Arrangement . . . . .	29
Figure 8. Microstructures for Various Heat Treatments of OFE Copper . . . . .	31
Figure 9. Stress Response as a Function of Cycles for the OFE Copper: AR, AR/IPS, HTA, and HTB Conditions . . . . .	34
Figure 10. Examples of Ultrasonic Records and Load Traces As Indicators of Initiation . . . . .	39
Figure 11. Evaluation of Surface Topography in OFE Copper Under Cyclic Loading . . . . .	43
Figure 12. Comparison of Monotonic and Half Life Stress Response for OFE Copper from Selected Tests: AR, HTA and HTB Conditions . . . . .	55
Figure 13. Trends in Microstructural Measures of Transient Behavior . . . . .	61
Figure 14. Fatigue Resistance of OFE Copper at 20 C in Flowing Argon . . . . .	67
Figure 15. Strain-Life Curves for a Variety of Steels . . . . .	71
Figure 16. Transients Evident in Dissipated Energy As a Function of Cycles . . . . .	72
Figure 17. Fatigue Resistance As a Function of Dissipated Energy . . . . .	72
Figure 18. Fatigue Resistance As a Function of $s_{mx}\Delta e^t$ . . . . .	80

## FOREWORD

This program was developed as a result of NASA's support of Battelle's unsolicited research proposal titled Nonlinear Damage Accumulation Criterion, submitted April 14, 1981. The proposal followed the concepts and approach outlined in a suggested research program of the same title submitted by Battelle on March 13, 1981, following discussion of the subject program with Dr. Gary Halford. The objective of the suggested program was to explore the viability of a nonlinear damage postulate that differs from the literature in the following significant way. Instead of assessing damage using the conventional resistance curve, the postulate asserted that the resistance curve is itself history dependent.

## INTRODUCTION

Tracking or predicting the damage state of structural components is essential to maximize utilization of materials and minimize losses associated with unscheduled downtime for repair or inadvertent failures. Some components are loaded in such a fashion that the maximum load encountered in service can be a priori estimated within a small margin of error. In such cases design against fatigue failure can be achieved by sizing components and selecting materials such that the design stress is less than the endurance limit using traditional concepts. That is "constant amplitude" cycling at the design stress would not cause failure. However, most structures and their components are not subjected to peak load limited situations which admit or ensure "infinite life" design. Rather the majority of the loadings are variable in amplitude (and, in general, involve a time varying direction of application). Many times the maximum loading cannot be predicted within a small margin of uncertainty, nor can the frequency of occurrence of very large loads be predicted. In such cases a variable amplitude damage analysis leading to "finite life" must be available to explore the extent to which such events limit life and serviceability.

Damage analysis under variable amplitude cycling requires three steps to be taken. First, ascending and descending segments of the stress strain history must be identified and matched, to construct closed loops similar to that formed under constant amplitude cycling. Second, damage done by a given event of loading must be assessed by comparing the number of times that event occurs with the resistance of the material to such events. This assessment thus involves a reference data base that characterizes this resistance. In the simplest framework - uniaxial stressing - this damage assessment requires a parameter that accounts for the effect of the mean stresses developed under variable amplitude cycling as compared to that of the constant amplitude reference data used in damage calculations. Finally, damage done must be accumulated in accordance with a criterion which specifies how the damage is integrated, and a running damage sum must be maintained and compared with a prescribed value that indicates when failure is predicted.

For more than 10 years the Japanese-developed rainflow cycle counting procedure [1] has found acceptance in damage analysis schemes, based on its successful use in such applications [2]. Subsequently, a number of numerical procedures have evolved for the purpose of forming cycles [3-7]. These procedures identify segments of hysteresis consistent with the material's plastic flow process, and have tended to displace rainflow procedures in damage analysis. In any event, a number of experience proven schemes are available for purposes of matching hysteresis segments to form cycles--the first step in damage analysis.

Numerous schemes are also available and continue to be developed to account for mean stress effects. The list of mean stress parameters is long. It includes one due to Morrow [8], one due to Smith et al [9] and variants or alternately developed forms similar to that of Smith et al [10-11] and others [12]. While successes are claimed in the literature for all mean stress parameters, the fact that such parameters continue to evolve indicates shortcomings exist in this aspect of damage analysis. Regarding the last aspects of damage analysis--damage assessment and accumulation--numerous studies illustrate the controversy and uncertainties involved with linear damage accumulation (e.g.[13]) whereas the subject of damage assessment has laid virtually untouched.

The mainstream of current technology continues to track the damage state by assessing and accumulating increments of fatigue damage on a cycle-by-cycle basis according to the Palmgren-Miner linear damage hypothesis. Studies have consistently shown the shortcomings of this hypothesis in the context of comparisons of observed life and life based on a linear damage calculation. Indicated errors are either conservative or nonconservative, sometimes by as much as a factor of 10 [14]. While studies have demonstrated errors as a consequence of the hypothesis, few if any have attempted to isolate the cause of these errors. Pertinent data indicate that, even when crack nucleation and crack growth damage are dealt with independently and cyclic, history dependent, mean stresses are accounted for, the linear accumulation hypothesis is still significantly in error when implemented with a linear assessment scheme.

The objective of this research was to develop an understanding of, and initiate formulation of an analytical model for damage analysis that reflects observed nonlinearities. It was desired that this model be sufficiently simple, so as to permit its use in tracking the damage state in metallic components subjected to a wide range of service histories, eventually including elevated temperature.

#### APPROACH AND SCOPE

While much data exist that indicate the inadequacies of the linear hypothesis, none of these data were developed as a result of an experimental program designed to fully explore and isolate the causes for the inadequacies. For this reason, the damage accumulation process is ill-understood at both the phenomenological and microstructural levels. The approach adopted for this program has been to perform a series of experiments designed to develop phenomenological and microstructural information regarding damage accumulation that facilitate evaluation of the utility of the nonlinear postulate. Given the fact that a new approach to damage analysis is envisioned, the scope of this research has been restricted to a preliminary study designed to explore the potential utility of the nonlinear analysis postulate.

Because little is known about damage accumulation, every effort was made to isolate the process from the various factors known to influence the damage rate - except for those being directly considered. For this reason, uniaxial specimens were used to avoid multiaxial stress effects. To avoid the complex interplay between strengthening mechanisms, a relatively simple material was preferred. For this reason, OFE\* copper was used; the material was taken from one bar from one heat.

To avoid the uncertainty in dealing with both nucleation and growth damage, this study focused on nucleation. ("Nucleation" is defined on page 10.) This has been achieved by using a smooth axial specimen designed such that most of its life is spent developing cracks of the size defined as nucleation. Finally, to avoid cycle dependent mean stress relaxation and the influence of mean stresses on the damage rate, the experiments have been designed such that unloading from tension or reloading from compression following sequenced blocks and overloads induced a small mean strain, rather than a mean stress. Small mean strains are considered not to be of much consequence for the type of study reported herein.

After isolating the problem as just detailed, one is left with the conclusion that the shortcomings in the linear hypothesis are due to the history dependence of the damage rate process. It is asserted that this dependence is manifest in terms of changes in (1) the bulk microstructure and (2) the surface topography and near surface residual stresses.

Changes in the microstructure are associated with hardening or softening, and occur in the bulk until decohesion in persistent slip bands and crack nucleation occurs. Thereafter, they are confined to the crack tip. It is postulated that a particular microstructure forms in the reference constant amplitude data base used in conjunction with the linear damage hypothesis in predicting damage under variable amplitude loading. It is further postulated that this microstructure may differ at a given damage (life) fraction from that developed under variable amplitude cycling. It is known that the fatigue

---

\*OFE denotes oxygen free electronic grade copper--the material is discussed later in the Experimental Details section.

resistance of a material changes with microstructural changes that are manifest as changes in hardness/ductility. For this reason, it is asserted that the baseline used in damage analysis should change to reflect history dependent changes in hardness/ductility associated with cyclic hardening or softening due to large or small load levels encountered in a given strain history. Because cumulative plastic strain is a measure of both hardening/softening and the bulk micro-structural state, it is asserted that this parameter may provide a very convenient basis to track the history dependence of the damage process. Cumulative plastic strain is already tracked in computer-aided damage analysis procedures. Therefore, accounting for the history dependence of the damage process to such procedures should not be too difficult.

With regard to surface, the character of the surface topography and surface residual stresses also reflects the history. Consequently, the evolution of surface residuals and roughening associated with slip step formation through cyclic plastic flow, can also be tracked in terms of cumulative plastic strain. Based on prior work, there appears to be a minimum level or threshold in the development of surface slip steps, after which slip band decohesion occurs and crack nucleation and growth ensues. Often the role of surface roughening is thought of in the context of mechanical notch effects. Consequently, until a notch forms, there is no effect - thus tentatively explaining the expected apparent threshold.

It is asserted that the just detailed history dependence of the damage process leads to the observed inadequacies in the linear history independent hypothesis. An experimental program designed to pursue bulk and surface manifestations of this history dependence in a preliminary fashion has been developed and performed. The results have been analyzed to facilitate evaluation of this postulate, and identification of controlling phenomenological parameters for the data developed. The approach adopted in this study to develop a history dependent damage theory, therefore, has involved a series of key experiments and analysis to identify the character of physically based damage theory. Results of this preliminary study follow in sections dealing with Damage Analysis, The Damage Postulate, Experimental Aspects, Results and Discussion, Examination of the Damage Postulate, Summary, and Conclusions.



## DAMAGE ANALYSIS

### Concepts Involved in Damage Analysis

#### Damage

Damage is herein taken as the progressive change in a material's microstructure, that eventually culminates in the nucleation and growth of cracks, due to the localized action of reversed microplastic strain and tensile stress. Thus the damage process involves the nucleation and growth of cracks. During the nucleation stage the damage process occurs at a scale strongly affected by the random nature of the microstructure, suggesting that damage models at the micromechanics scale should be probabilistic. Furthermore, because the process occurs at a microlevel it is difficult to track. Fortunately changes that lead to nucleation apparently also result in changes in the bulk deformation behavior and in the character of the material's surface. This coupled with the fact that bulk deformation parameters are easily measured has led to their popular use as measures of the damage per cycle.

After nucleation fundamental studies indicate that the advance of a crack is a simple geometric consequence of the slip at the crack tip. Measures of damage related to crack advance therefore may be provided in terms of the propensity for slip at the tip (local strain, etc., related to far field stress and crack geometry) or geometric crack variables (CTOD, crack length, etc.). Damage can be characterized by continuum mechanics parameters before nucleation, whereas after nucleation the mechanics of cracked geometries is required. Clearly then when initiation and propagation are being considered in a fatigue life prediction there is a "grey" area wherein a transition must be made, based on crack size, from the initiation analysis scheme to the propagation analysis scheme. The crack size at which the transition is made is based on one's assessment of the size of crack at nucleation. Fortunately, with an appropriate propagation analysis scheme the error made as a result of the selection of the crack size at the "just initiated" crack is small.

## Damage Parameters

The concept of a damage parameter is introduced into damage analyses because the reference data used to assess the damage done by a variable amplitude event may not be developed under identical conditions. In general, stress-strain path/multiaxiality, temperature, environment, loading rate, etc. may differ between the component being analyzed and the reference data. Thus a damage parameter, defined as an analytical (or empirical) relationship which establishes the link between the complex damage process in the component and the simpler situation for the laboratory reference data, is required.

For the present case the only potential difference between constant amplitude reference condition and variable amplitude loading is mean stress.\* Thus only a "mean stress" damage parameter is required and discussed. Damage parameters used in this study have the form [12]:

$$D = s_m \Delta e^t + \Delta s \Delta e^t, \quad (1)$$

where  $s_m$  is the mean stress and  $\Delta s$  and  $\Delta e^t$  are the stress and total strain ranges respectively. This parameter was selected because it has been shown useful in correlating data developed under both complex multiaxial proportional loading [12,16] and uniaxial mean stress conditions [17].

Simpler uniaxial forms for the parameter include the product  $\Delta s \cdot \Delta e^t$  in the absence of mean stress effects. This product is equal within a scalar multiplier to the denominator of the Neuber parameter, which is popular in notch analyses [18-19]. It can likewise be manipulated to yield

$$\frac{D}{\Delta s} = \Delta e^e + \Delta e^p, \quad (2)$$

---

\*While it was sought to avoid mean stresses through the use of specific strain histories in the variable amplitude experiments, small mean stresses did develop in some instances. Thus a mean stress parameter was required. In cases where mean stresses have been avoided, this has been accomplished with the introduction of small mean strains. Mean strain may be a factor under certain conditions - for example forming prestrains [15]. However, the small mean strains introduced to avoid mean stresses in the present study were very small and thus their effect was ignored.

in which the right hand side is equal to the sum of elastic and plastic strain ranges used by Morrow [20] to characterize fully reversed (zero mean stress) fatigue data. For linear elastic conditions the parameter can be manipulated to yield a parametric form which has units of stress:

$$D_1 = (DE)^{\frac{1}{2}} = (s_m + \Delta s)\Delta s^{\frac{1}{2}} \quad (3)$$

or

$$D_1 = (DE)^{\frac{1}{2}} = s_{mx} \frac{(3-R)(1-R)}{2}^{\frac{1}{2}}, \quad (3a)$$

where  $s_{mx}$  is the maximum stress in a cycle and  $R$  is the stress ratio. This form is similar to one variant of the parameter proposed by Smith et al [9]. For linear elastic fully reversed cases one obtains  $D_1 = \Delta s^2$ , a form similar to the Basquin relationship [21] when correlated with fatigue data. Finally for situations where the inelastic strain dominates ( $\Delta e^t \approx \Delta e^p$  and  $s_m \approx 0$ ), one obtains  $D \approx (\Delta s)(\Delta e^p)$  or  $D \approx C (\Delta e^p)^{n'+1}$  which, when correlated with fatigue data, is a form similar to the Coffin-Manson relationship [22,23]. In these respects the parameter given in Equation (1) has a form operationally similar to several of the experience proven parameters, when applied to specific simplified situations that these previously developed parameters had been developed for. Its utility has been demonstrated elsewhere for a broader more general set of situations [12,17]. The concept of the damage parameter is illustrated by its application to correlating fatigue data for a typical case in Figure 1.

### Similitude

For a damage parameter to provide the link between the situation at a critical area in a component, all of the factors which impact on the damage per cycle at that location not embedded in the reference data must be accounted for by the damage parameter. Similitude means that equal values of the damage parameter applied at two critical locations\* results in equal lives

\*Also, there must be similitude between the materials at these locations. In a statistical sense, chemistry, phase(s), orientation, and other microstructural variables must be equal. It follows that there is a minimum volume of material needed to develop this statistical homogeneity.

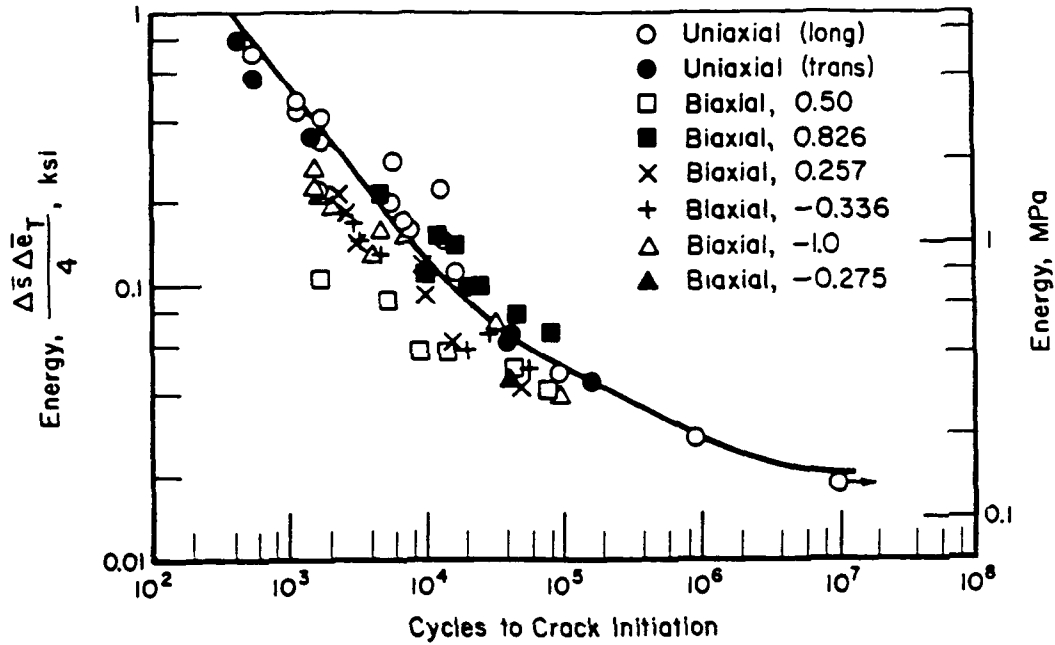


FIGURE 1. TYPICAL APPLICATION OF A DAMAGE PARAMETER USED TO CONSOLIDATE MULTIAXIAL FATIGUE RESISTANCE OF 1015 MILD STEEL -  $\Delta \bar{s}$  AND  $\Delta \bar{e}_T$  ARE EQUIVALENT UNIAXIAL MEASURES OF STRESS RANGE AND TOTAL STRAIN RANGE (AFTER (12))

to crack nucleation within statistical scatter at both locations. Obviously similitude between the damage processes at the two locations must be ensured if accurate predictions are to be expected. Similitude can be achieved most easily by demanding less of the damage parameter. This can be accomplished by using constant amplitude reference data that reflect the important component loadings - thermal, multiaxial mechanical, time and path dependent considerations being among the more difficult aspects to analytically account for. Clearly too, different damage parameters and reference data are required if a significant macrocrack growth stage exists in the component for a period different than in the reference data.

Similitude is a key aspect of any damage analysis, be it for nucleation or for macrocrack growth as detailed in Reference [24] and [25] which deal with crack growth and nucleation respectively.

#### Operational Definition of Nucleation

With respect to the above discussion, the focus here is on the nucleation stage established in terms of when bulk parameters indicate cracking. The operational definition of nucleation\* adopted herein is the life for which the back extrapolated asymmetric drop in the tensile load intersects the stable deformation response, as shown schematically in Figure 2. Calculations of "area lost" due to cracking indicate this definition is associated with surface cracks with a shallow aspect ratio whose depth is on the order of 50 to 200  $\mu\text{m}$ . Similar calculations indicate that a one percent load drop relates to a depth of 400  $\mu\text{m}$  and the often reported five percent load drop related to a depth of  $>1200 \mu\text{m}$ .

Experience with the above definition suggests that it typically indicates "nucleation" before continuous monitoring with a reflection ultrasonic scheme using a specimen geometry and transducer optimized for crack detection as detailed later in the section dealing with experimental results. The threshold for detection using that scheme is a depth of about 75  $\mu\text{m}$  for calibration specimens. Nucleation based on the above operational definition

---

\*Hereafter, the terms nucleation and initiation are used interchangeably.

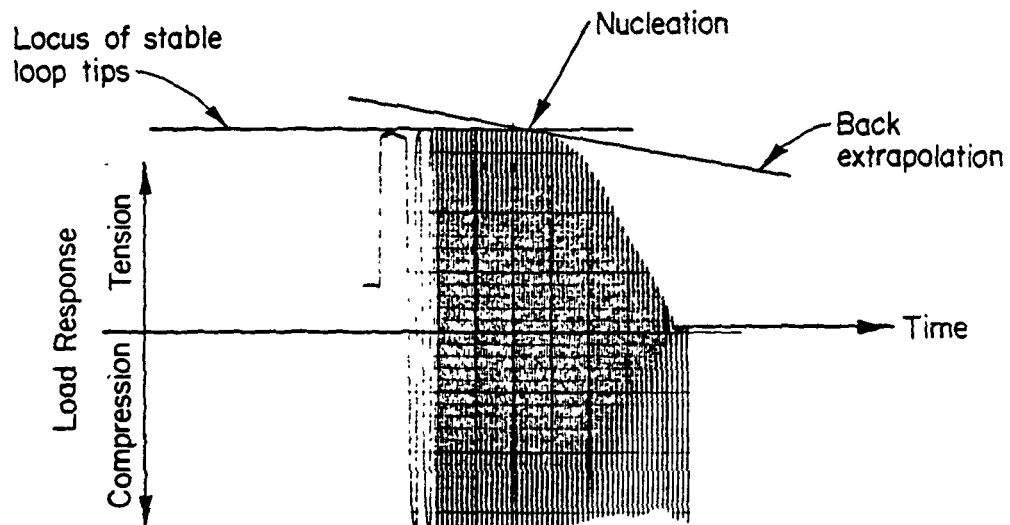


FIGURE 2. SCHEMATIC ILLUSTRATING THE BACK EXTRAPOLATION PROCEDURE TO DEFINE NUCLEATION (OFE COPPER,  $N_f = 853$  CYCLES)

also has been compared with results of surface studies made using single stage gold coated replicas interpreted at up to 5000X magnification in a SEM. This comparison detailed later in the section dealing with experimental results indicates nucleation defined as above using bulk parameters correlates well with the onset of growth of Mode I cracks from the much earlier formed and subsequently intensified Mode II and Mode II/Mode I slip band extrusions and long-shallow shear oriented surface cracks.

### Phenomenology Relevant to Damage Analysis

The literature on damage analysis indicates either linear damage accumulation, as suggested by Palmgren [26] and by Miner [27], or some non-linear scheme (for a summary see [13]) is employed. In virtually all cases a single curve is used to characterize the materials damage resistance--as for example either a stress-life or a strain-life plot. The essence of all procedures is to compare cycles applied in a variable amplitude history to the damage resistance observed under constant amplitude cycling. It is therefore instructive to examine the constant amplitude situation to see if some insight as to the character of a damage theory can be extracted.

First, under constant amplitude control, the response parameter changes as a function of cycles and the driving force for transient action--inelastic strain. Under strain control, hardening or softening occur as does mean stress relaxation. Under load control hardening and softening also occur but given the unstable nature of the control condition, cyclic creep may intervene to cause premature failure. So long as one deals with constant amplitude cycling, knowledge of the magnitude of the control parameter is all that is required to specify the life within statistical bounds. This is because changes in the response parameter which occur do so in similar fashion from test to test. For strain control,  $\Delta e^e$  and  $\Delta e^p$  change so that the ratio  $\Delta e^p/\Delta e^e$  varies on a cycle by cycle basis even though  $\Delta e^t$  remains constant. Thus, as Equation (2) indicates stress, a factor for consideration in more general situations, can be factored out to yield elastic and plastic strain as the sole basis to characterize fatigue resistance for a fully reversed situation.

### Assumptions

For constant amplitude cycling it is reasonable to assume that up to nucleation each cycle in the history does an amount of damage that is proportional to the value of the bulk damage parameter on the cycle. Because these data serve as a basis for variable amplitude damage analysis, transients that could be ignored in selecting the damage parameter for constant amplitude cycling no longer can be ignored. The implication is that  $\Delta e^t$  may be an adequate basis for comparing constant amplitude data but in general is an inadequate basis for characterizing the driving force for damage under block sequence or variable amplitude cycling.

The just stated assumption means that each cycle of a history for which the value of the damage parameter is the same (damage parameter control) causes an equal amount of damage. When integrated over the history, one obtains a measure of the material's resistance to damage. Clearly one could integrate the damage per cycle over the history using any weighting per cycle he chose. However, the phenomenology does not indicate any one cycle is more damaging than another. Thus it is assumed that damage per cycle is equally weighted over the life to nucleation. This equal weighting leads to a linear accumulation criterion. Applying this same logic to a constant amplitude test done in strain control leads to a nonlinear weighting per cycle if strain range is used as the damage parameter. This weighting follows from a comparison of the values of the damage parameter given respectively by Equations (1) and (2). For materials which stabilize quickly the weighting affects only a few cycles, whereas for materials such as RQC-100, which exhibits exponential softening [5], the weighting affects much more of the life.

One can derive empirical weightings to modify the linear accumulation criterion to suit the damage parameter employed such as just illustrated. However, it is much simpler to couple a more general parameter with the linear accumulation assumption and assess and integrate damage on a cycle by cycle basis for constant amplitude loading. Extending this approach to variable amplitude loading requires a second assumption--that closed loops\* under

---

\*While closed loops are discussed this assumption and the one just prior could have been equally stated in terms of reversals.



constant amplitude loading do the same amount of damage as their variable amplitude counterparts. It is instructive to look briefly now at phenomenology related to damage assessment.

### Important Questions

Some now consider it well established that a material's long life endurance relates to hardness (strength) while its short life resistance relates to its ductility in view of published correlations (e.g., [28]). Transient action develops under cyclic loading (e.g., [20]) for which it seems rational to postulate that the bulk hardness and ductility depend on the cyclic history. Also there tends not to be a saturation or steady state under variable amplitude loading [29]. Furthermore variable amplitude stress histories are not the same as that of the constant amplitude results used as reference data in damage analysis. For example, in the long life regime cyclic hardening would in this context enhance the material's resistance to damage and require a nonlinear assessment of the damage done based on the imposed history. Therefore it seems reasonable to ask: should the reference data used for damage assessment reflect the history dependent hardness/ductility state of the bulk component material in the vicinity of nucleation?

Second, it is reasonable to postulate in view of published data (e.g., [30]) that the surface of a material roughens as damage localizes and eventually tends to concentrate in areas from which cracks nucleate. Clearly the surface character may evolve differently under variable amplitude loading as compared to the constant amplitude results used as reference data in damage analysis. Given that surface roughening acts as a notch one might expect based on the literature (e.g., [31]) that in the long life regime the fatigue resistance is strongly reduced once a notch of a threshold size is developed. Again damage assessment is nonlinear, depending on the history imposed. Therefore it also seems reasonable to ask: should history dependent surface topography be embedded in damage assessment and if so how?

Third and finally, surface grains are free to deform under plane stress at strain levels below their constrained interior counterparts\*.

---

\*In this context, surface means the plane stress surface layer.

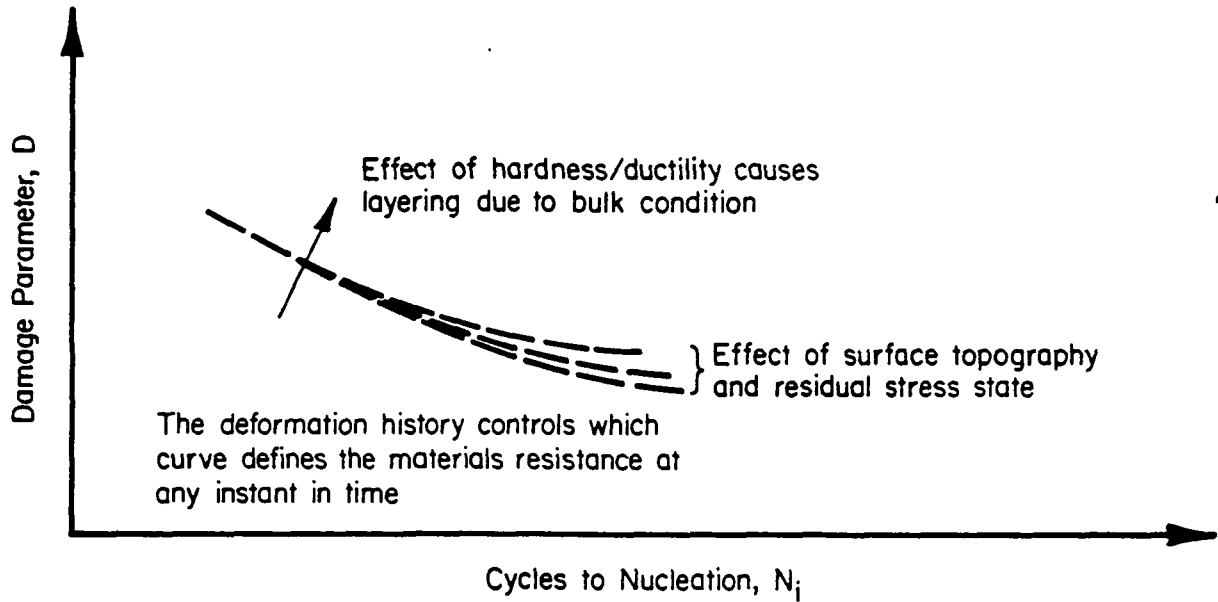
Therefore it is conceivable that, for a narrow window of cyclic strains within the low strain, long life regime, the surface could yield in tension or compression and be constrained by the elastic interior. In turn this would set-up surface residual stresses that could either retard or enhance the damage process depending on the sense of the reversal that causes yielding. (Pangborn [32] discusses this aspect in the literature.) Related to this are grains most favorably oriented for slip which may also yield and be constrained by their unyielded counterparts in a very narrow window in strains, biased again to the low strain long life regime. While the sign of the residual stress that develops depends on the sense of the strain that first caused yielding, fatigue is a selective process and will seek out grains in which damage will accumulate most rapidly. Under constant as well as under variable amplitude loading grains may be expected to yield under both tensile and compression going cycles, with a few exceptions. Thus the effect of compression yielding creating tensile residual stress will always be observed in that it will reduce the life by locally enhancing the damage per cycle. But the effect of local compression residuals due to tension yielding will seldom be seen because cracking in other grains will intervene. In view of this it is reasonable to ask: should the character of surface residual stresses due to the loading history be imbedded in damage assessment.

#### THE DAMAGE POSTULATE

It is postulated that the nonlinear nature of the damage process arises through a history dependence of the material's fatigue resistance which depends on the bulk hardness/ductility, and the character of the surface topography and residual stress field. In this respect the nonlinear nature of the damage process involves damage assessment but not damage accumulation.

The essential features of the postulate are presented in Figure 3. Experiments performed to evaluate the potential utility of this analysis framework are now presented.

A Schematic of the General Situation



Damage Analysis at Specific Instants in Time

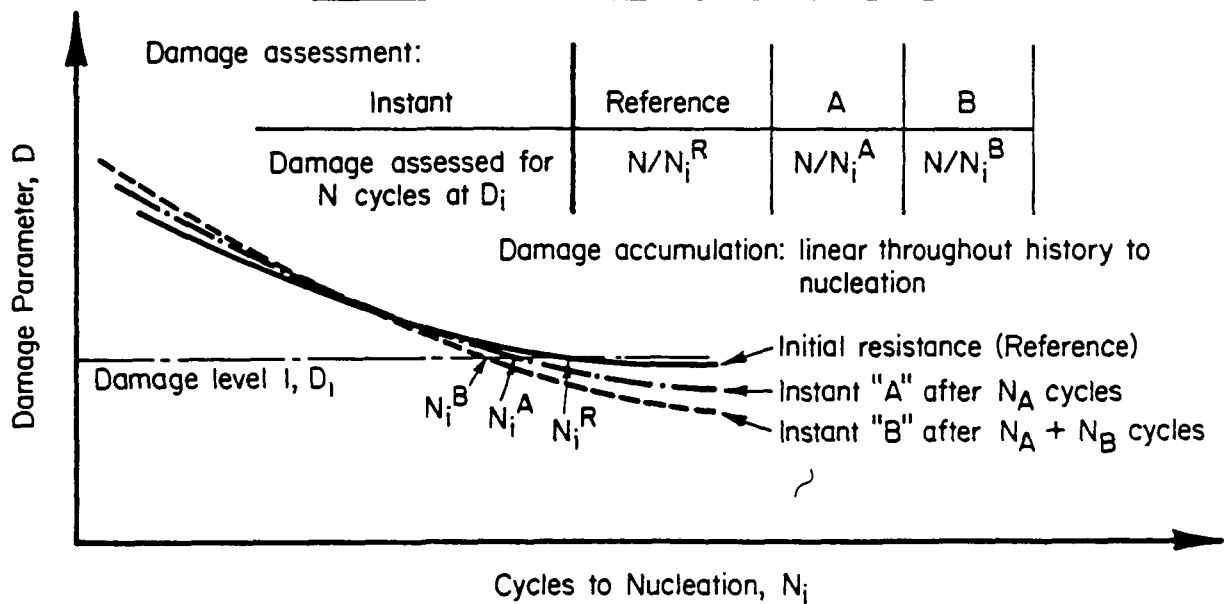


FIGURE 3. ESSENTIAL FEATURES OF THE DAMAGE ANALYSIS POSTULATE

EXPERIMENTAL ASPECTSTest MatrixData Requirements

Meeting the objectives of this preliminary study required data be developed to explore each of the key features of the damage postulate. To this end the experimental program developed data to determine if (1) hardness/ductility, (2) surface residuals and (3) surface topography develop in a characterizable fashion as a function of history. Thereafter, data were required to determine if there was a history dependence of the fatigue resistance and whether such a dependence could explain the apparent nonlinearity in damage analysis under variable amplitude loading.

Detailed evaluation of the postulate required data to explore each of the bulk and the surface contributions in an uncoupled fashion over a range of lives that embraced a range of lives both well above, through, and well below the transition life. Studies of the bulk needed to introduce bulk changes, and then isolate their effect by removing the surface after pretreatment. Studies of the surface topography needed to develop the surface morphology desired using various prestrain histories and then relieve all mean stresses and hardening either through a decremental step loading and/or heat treatment. Surface residual stresses needed to be studied either directly via measurement or indirectly via their effect on life for comparable bulk states and surface topographies.

Detailed study of damage evolution and the postulate advanced, while useful and warranted in a fundamental sense, would involve far more data development than that needed to explore the viability of the concepts that underlie the postulate. This coupled with the novel history dependent resistance curve central to the postulate suggests that the viability of the postulate should be explored in a much reduced study. Finally it is often easier to identify trends which if developed in the data for critical experiments indicate a postulate is either viable or questionable on empirical or physical grounds, than it is to prove a postulates value. For this reason the

simpler approach was adopted. Consequently, if the postulate would be shown to be consistent with the phenomenology, it will be argued that the postulate is viable, and warrants further study as a basis to characterize the nonlinearity in damage analysis.

#### Approach to Meet Objectives

The postulate advanced followed from consideration of the phenomenology of damage which led to three questions. The purpose of the experiments performed was to develop answers to these questions through study of three key aspects namely, the existence of the implied correlation of microstructural changes with bulk deformation parameters, and the evolution of surface topography and stress-strain history. Thereafter the existence of history dependent fatigue resistance curves is pursued.

The correlation between microstructural changes and changes in bulk deformation parameters can and has been explored at many levels. Studies at a very microscale address dislocation structures, as presented in the notable works of Mughrabi [33], Laird [34] and others, and as summarized for example by Kocanda [35]. It is changes at that level which are shown to relate to eventual cracking and in turn are postulated to relate to bulk measures such as stress. Changes in microhardness reflect the integrated changes in microstructure over a small volume of material and in turn these relate to changes in dislocation behavior. Consequently, changes in microhardness measurements reflect changes at the dislocation level. Therefore, a correlation of changes in bulk measures with changes at the dislocation level can be demonstrated by directly comparing the measured change in microhardness with the corresponding change in stress under strain control. For the postulate to be conveniently implemented, these changes must be a function of cumulative plastic strain  $\Sigma \epsilon^P$ , and be independent of how  $\Sigma \epsilon^P$  is introduced.

Correlation between surface topography and stress-strain history can be explored by tracking the surface via replication under the action of various histories. In the present study this was conveniently accomplished using single stage replication performed on samples tested under selected combinations of strains and cycles. The procedure involved replication after each

major sequence event as well as at intervals equal to one tenth of the expected life. The replicas were then examined in an SEM and the results documented at 50X, 250X, 500X, 1000X and 5000X magnification. Again for the results of this study to be useful they must correlate uniquely with some parameter such as  $\Sigma e^P$  or some other related sum that includes stress.

Surface stress state effects can be examined in terms of the life obtained under selected sequences over a range of strains. This study explored the possible effects of surface stress states by starting tests in opposing directions - one in tension and one in compression. Because the extensive bulk inelastic action that develops at higher strains leads to a homogeneous deformation state that washes out any microresiduals should they develop, consideration of this possible effect began at the lowest strain being considered. If there was an effect, the test started in tension should survive longer than that started in compression for the same fully reversed cyclic strain. If this result developed, testing would explore higher strains, until the effect washed out. In all cases, the behavior of the surface residual stress (if it is a factor) should be characterized as a function of the imposed history.

The final aspect of the postulate examined was the implication that a material's resistance to damage is history dependent, beyond the sequence related effects of surface roughening. Recall, as hypothesized earlier, that bulk changes in stress relate to changes in microstructure which in turn relate to damage. This means that the material evolves in its hardness or ductility so long as microstructural changes, evident in terms of changes in bulk parameters, are occurring. Also, it means that if different stress levels develop for the same strain range after different deformation histories in a given material, then differing amounts of damage per cycle develop even though the ensuing strain history is the same. Consequently if different fatigue resistance curves can be developed for the same material in differing initial states of hardness/ductility one can conclude that a sample of material exhibiting transient response will also exhibit differing fatigue resistances over its life. Because transient behavior is history dependent in general, one could also conclude that the fatigue resistance is history dependent, consistent with the postulate.

History dependence of a material's fatigue resistance was examined as just suggested by comparing the fatigue resistances of a material in several different initial hardnesses/ductilities. Results were developed by testing samples prepared in one of four hardnesses (developed by heat treating or mechanically working the as-received material). Testing was done at one of three identical total strain levels, designated as  $\Delta\epsilon_1$ ,  $\Delta\epsilon_2$  and  $\Delta\epsilon_3$ , selected to cause nucleation at about  $10^3$ ,  $10^4$ , and  $10^5$  reversals. These same levels were used throughout the study.

### Test Plan

The test plan followed is detailed in Table 1. It embraced a total of 26 tests. Of these, 10 were targeted for constant amplitude cycling while the remainder were subjected to some form of strain history. Additional samples were committed to establish optimum conditions for ultrasonic detection of nucleation, as well as for calibration of the ultrasonic output with crack size.

## Experimental Details

### Material and Specimen

The material used in this study was specified to be oxygen free electronic (OFE) grade copper. Copper was used because it provides a single phase model material for which the inelastic aspects, indicated by the postulate to control nonlinearities in damage analysis, will be accentuated. The material was obtained in the form of 25.4 mm diameter bar, a total of 20 kg being purchased. The material's reported composition was verified via spectrographic analysis as (in ppm) Pb:3, Zn<1, Te<1, Se<1, P:1, O:2, S:12, Hg<1, Cd<1, Bi<1, Cu: balance. Some samples also indicated traces of silver. In view of the chemistry, the material met the OFE copper specification ASTM: F-68(77). Trace elements account for ~13 ppm so that the sample was 99.9987 percent pure copper. Mechanical properties determined by the supplier were a 297 MPa yield strength (0.5 percent offset) with an average elongation of 24

TABLE 1. TEST PLAN

No. of Tests	History	Purpose
9	Constant Amplitude (CA) <sup>a</sup>	Develop data for differing initial hardness/ductility states
1	Constant Amplitude <sup>b</sup>	Examine effects of surface residual stress
6	Incremental Prestrain (IPS) <sup>c</sup>	Develop a different initial hardness/ductility state by mechanically action
8	Initial Overstrain (IOS) <sup>d</sup> with Decremental Prestrain (DPS)	Develop differing initial surface topographies
2	Block Cycling (BC) <sup>e</sup>	Develop data to test viability of postulate

- (a) CA fully reversed strain cycling starting in tension
- (b) CA fully reversed strain cycling starting compression
- (c) IPS consisted of a gradually decrementing block of 30 reversals to zero strain from  $\Delta e_1$ , followed by a gradually incrementing block to the desired peak strain for the test
- (d) IOS/DPS consisted of an initial CA overstrain at  $\Delta e = 0.0204$  for N cycles as indicated case by case, followed by a reversal decremental sequence to zero strain, followed by CA cycling
- (e) BC consisted of alternating blocks of low high or high low CA straining as follows:  $10^4 @ \Delta e_3 / 10 @ \Delta e_1$ , repeated to failure or  $10 @ \Delta e_1 / 10^4 @ \Delta e_3$ , repeated to failure



percent. These properties indicated the material provided was cold worked between 20 and 40 percent. The grain size was ASTM 2½ to 3.

The specimen design involved a trade-off between the shape and size desired for low cycle fatigue testing and the requirements of ultrasonic crack detection.

An optimum design from an ultrasonic viewpoint involved consideration of limiting beam spread, the desire to achieve plane waves, and the desire to locate the transducer as close to the gage section as possible to enhance crack detection sensitivity. One final consideration involved choosing a geometry to minimize noise from reflections outside the gage section. To this end a transducer optimized to the material and geometry was designed and fabricated by Search Unit Systems Incorporated.\* The transducer was located nearer the gage length by burying the transducer in an access hole in one end of the specimen. The distance from the gage section, the diameter of the transducer, and the shape of the specimen were chosen to limit the amount of signal reflected from outside the gage section that would be returned to the transducer during the time period the signal would return from the gage section. These considerations led to the gage section and transition shoulder geometry shown in Figure 4.

All specimens were machined in a tracer lathe using standard shop procedures for copper. Samples were turned in the hardened as-received conditions using progressively finer cuts. The last 0.5 mm of radius was removed using two cuts of .1 mm, two cuts of 0.05 mm and eight approximately equal cuts of about 0.012 mm. This procedure was used to minimize any residual stresses induced by machining, even though enough inelastic action was expected in the tests to quickly wash out their effects. A total of 36 specimens were machined for the program. Of these 4 were used in various facets of testing the ultrasonic procedure. The remainder were committed to mechanical testing.

---

\*Search Unit Systems, Inc.  
San Antonio Texas, 78228  
Attn: Mr. K. Briers.

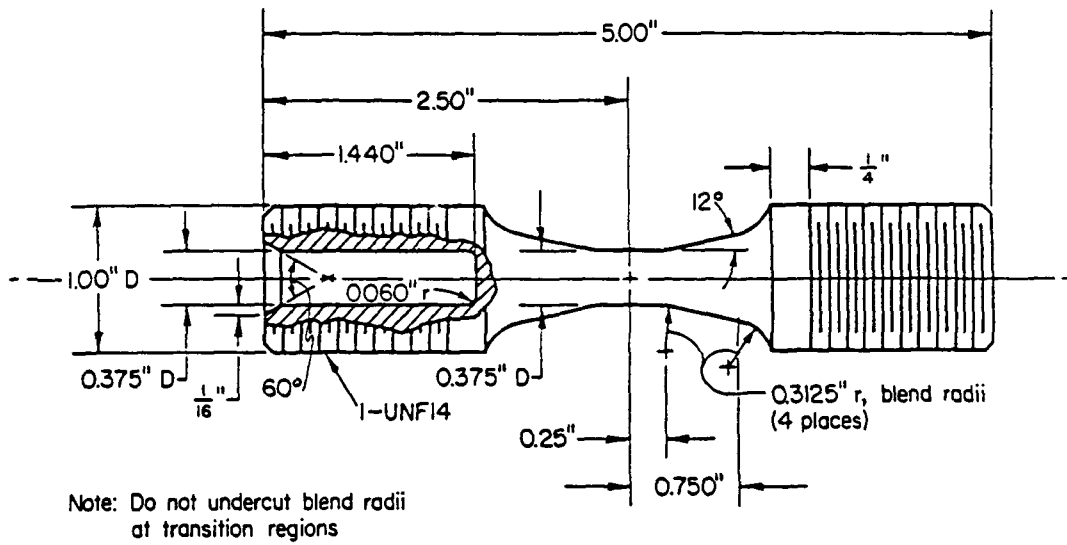


FIGURE 4. AXIAL FATIGUE TEST SPECIMEN (DIMENSIONS IN INCHES)

### Apparatus and Procedure

All mechanical testing was performed in one commercially available closed loop servocontrolled electrohydraulic test system. All testing was performed in strain control at frequencies ranging from 2 Hz for the smaller strains to 0.2 Hz for the highest strain. Temperature rise measured in a benchmark test was less than 4 F under these conditions. Specimens were subjected to a variety of essentially fully reversed axial straining sequences primarily using a sinusoidal pacing function. Strain was controlled in the 12.52 mm long gage section using a clip-on extensometer calibrated at the start of and three times during the program to ASTM Class B<sub>1</sub>. Load was monitored in all tests using a load cell mounted in series with the specimen. Calibration of the load cell was performed prior to and verified once during the test program. The load cell was observed to be accurate and linear within 0.1 percent of the operating range used in the present program. All recording devices were calibrated at the start of the testing.

All specimens were gripped in a fixture that featured a liquid/solid Cerrotru alloy grip which served to minimize stresses when mounting the specimens. Prior to starting the test program, the alignment was adjusted to minimize bending strains to less than  $\pm 5$  percent of the imposed strain, as required by ASTM E606. Before commencing with the experimental program, the closed loop system was tuned to allow testing at the optimum system gain. The procedure used for each test follows: after mounting the specimens in the upper grip, the load train was closed by freezing the liquid-solid grip under load control conditions. Maintaining the system at zero load, the extensometer was mounted and zero suppressed and all recording devices were activated and zero suppressed. The system was then shut down and strain control selected. The system was then reenergized and allowed to stabilize before strain cycling. In tests where the system had to be periodically shut down and restarted (such as for surface damage replication), care was taken to unload and thereafter reload without inducing spurious mean stresses. Monotonic and cyclic deformation response was recorded continuously during the first ten cycles and at logarithmic intervals thereafter on an X-Y recorder. Both load and ultrasonic output were continuously recorded on a time-based, high-speed strip chart recorder.

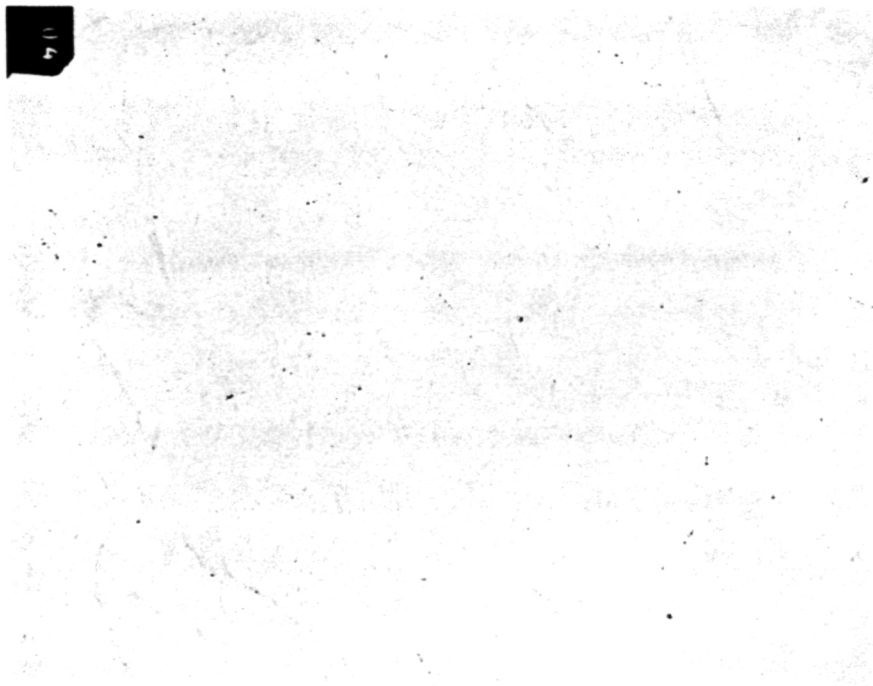
Initial tests were conducted in an ambient air environment at 40 percent relative humidity ( $\pm 5$  percent) and 20 C ( $\pm 1$  C). But some uncertainty as to the value of these initial tests existed in that intergranular (IG) cracking occurred whereas a ductile initiation was anticipated as well as required for this study. Examination of the failed specimens showed evidence of  $\text{Cu}_2\text{O}$ , as is apparent in the randomly located dark areas shown in the micrograph in Figure 5(a). Furthermore, the near surface grain boundaries were preferentially decorated by  $\text{Cu}_2\text{O}$ , as shown for example in Figure 5(b). Concern for the presence of the  $\text{Cu}_2\text{O}$  developed when further study showed crack initiation in these tests occurred preferentially at grain boundaries, and continued along grain boundaries. Examples of two such cracks are shown in Figures 6(a) through 6(d) at 350X and 1500X magnification. Such brittle initiations jeopardize meeting the objective of these tests--study of nonlinear history effects which according to the postulate arise due to inelastic action culminating in ductile initiation. After identifying that IG cracking associated with  $\text{Cu}_2\text{O}$  observed in grain boundaries near the surface was occurring, sample specimens of the copper bar were tested against the standard acceptance criteria for oxygen free copper\*. The tests indicated that the samples met the standard for OFE copper. Consequently the  $\text{Cu}_2\text{O}$  evident near the surface of specimens was believed to be forming during the cycling. To circumvent the IG initiation (without a detailed study of its cause), all subsequent tests were performed in a 99.999 percent flowing argon atmosphere at a back pressure of one inch of mineral oil, with testing commencing after a 15 minute chamber purge. Whether or not oxygen entry during testing caused the observed IG cracking, the incidence of IG initiation and growth ceased once testing in Argon began. All results developed in this fashion showed uniform deformation in the gage section and ductile initiation, in accordance with the requirements of this study. A photograph of the test chamber and gripping arrangement used is shown in Figure 7.

---

\*The test consisted of examining a polished sample of OFE copper after etching to decorate the  $\text{Cu}_2\text{O}$  (red). Evidence of decoration below 75X magnification is defined as excessive  $\text{Cu}_2\text{O}$  and the material fails to qualify as OFE.

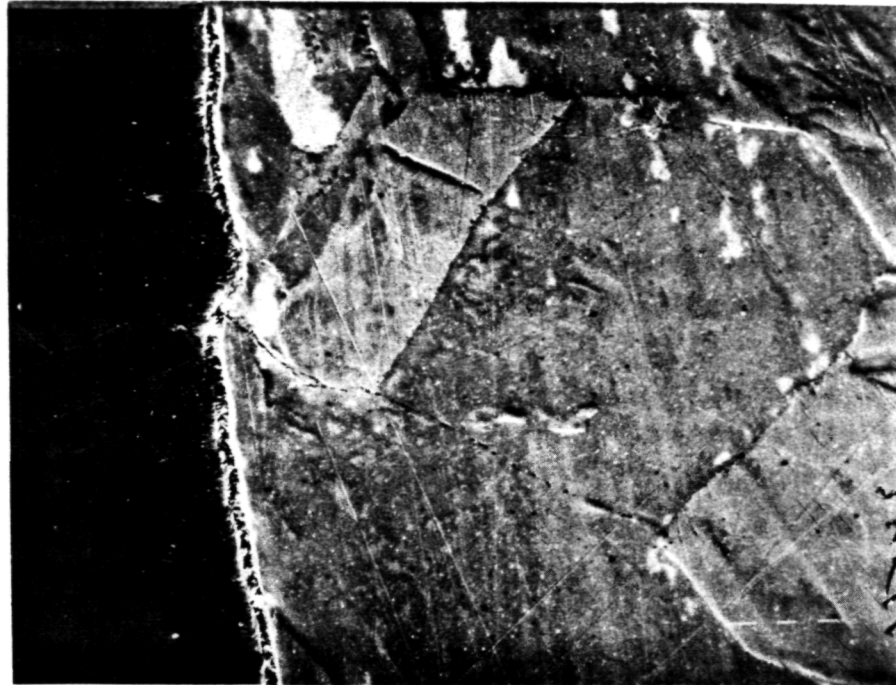
ORIGINAL PAGE IS  
OF POOR QUALITY

(a) View in bulk at 100X (7K776)



(b) View showing decoration near surface  
at 100X (7K777)

FIGURE 5. EVIDENCE OF  $\text{Cu}_2\text{O}$  FORMATION

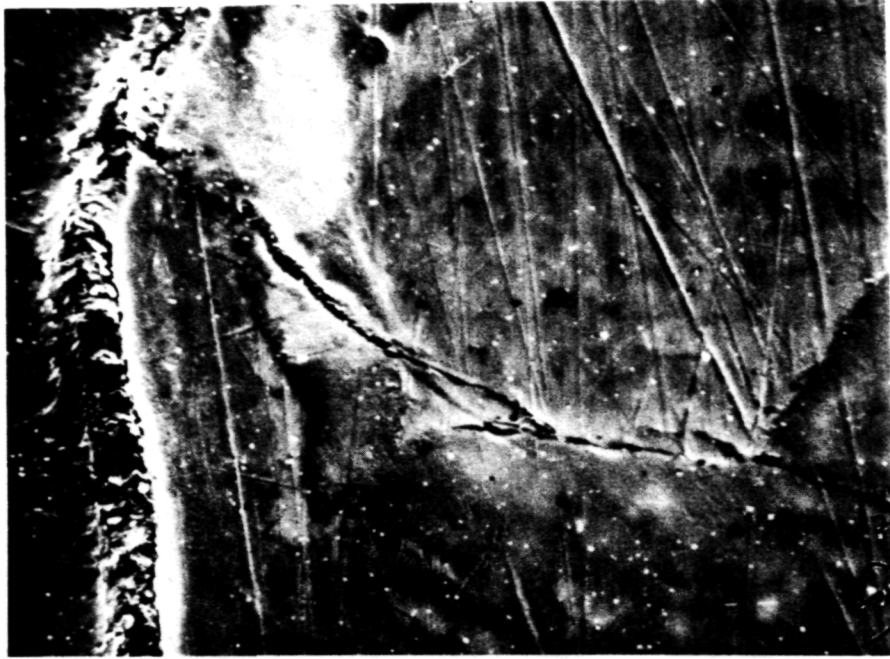


(a) IG initiation at surface - view A  
at 350X (SEM-34566)

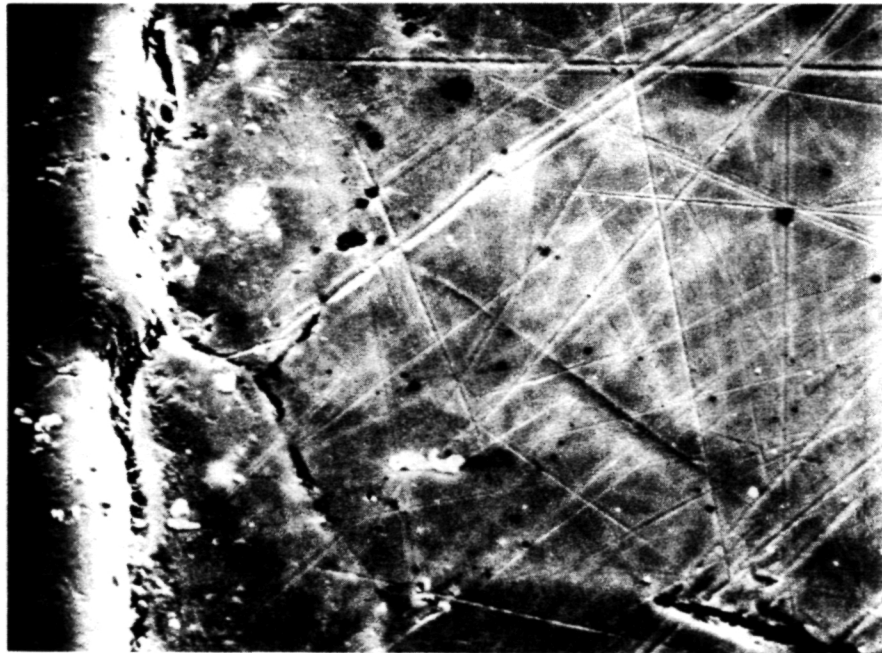


(b) IG initiation at surface - view B  
at 350X (SEM-34568)

FIGURE 6. EVIDENCE OF  $\text{Cu}_2\text{O}$  AND ITS APPARENT INFLUENCE  
ON INITIATION (SPECIMEN 2)



(c) IG initiation - View A at 1500X (SEM-34567)



(d) IG initiation - View B at 1500X (SEM-34569)

FIGURE 6. Continued

ORIGINAL PAGE IS  
OF POOR QUALITY

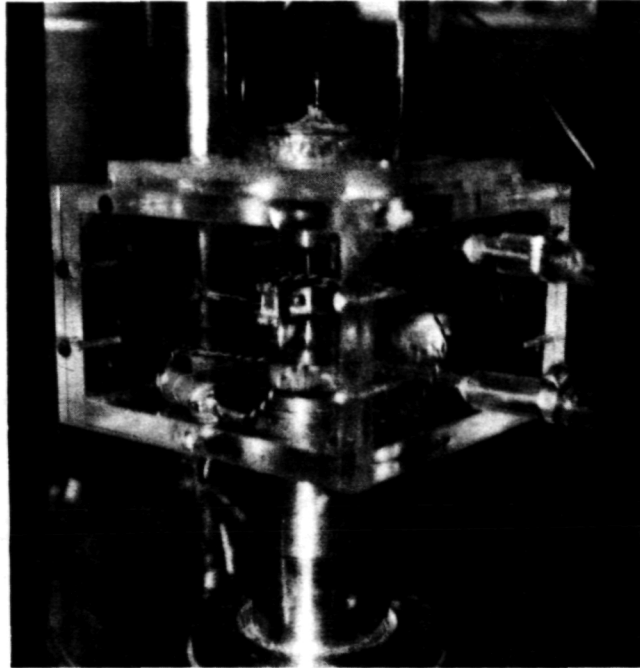


FIGURE 7. OVERVIEW OF TEST CELL AND GRIPPING ARRANGEMENT



## RESULTS AND DISCUSSION

### Material Characterization

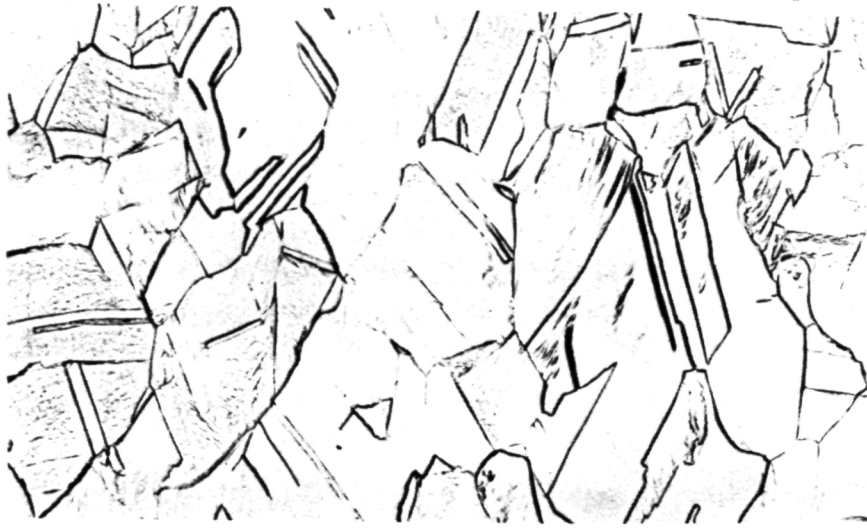
The OFE copper used in this study was cold worked between 20-40 percent and according to the suppliers certification had a nominal hardness of 87.5 on the Rockwell hardness F scale (HRF). A value of 87.5 HRF corresponds to a diamond pyramid hardness (DPH) value of 98. Hereafter, all hardnesses will be reported in terms of DPH values.

The microstructure of the as-received material was found to contain extensive deformation induced twins, as shown in Figure 8(a), and had a grain size of ASTM 2½ to 3. Because initial hardness/ductility of the material was a program parameter, samples of the as-received material were heat treated under a variety of conditions chosen with a view to decreasing hardness without radically changing the microstructure. Extensive recrystallization and in particular grain growth thus were undesirable. Study of the literature for copper base alloys (e.g., [36]) indicated major reductions in hardness could be achieved using anneals at 270 C, and that this would promote limited recrystallization and produce only nominal increases in grain size. To this end samples of the as-received (AR) material were annealed at 270 C\* for periods of 1, 5, 10, and 24 minutes denoted as HT1, HT5, HT10, and HTA. Microstructures that developed showed nominally no changes in grain size or twin morphology, as evident in Figure 8 parts (b)-(e). Grain sizes remained at ASTM 2½ to 3. Hardnesses measured 8 or more times developed the following mean/standard deviation DPH values for the condition noted: AR, 101.1/5.67; HT1, 102.64/2.06; HT5, 101.93/1.28; HT10, 100.68/1.08; and HTA, 103.58/4.27. In view of these data, there was no significant effect apparent in the microstructure or hardness due to these short term anneals.

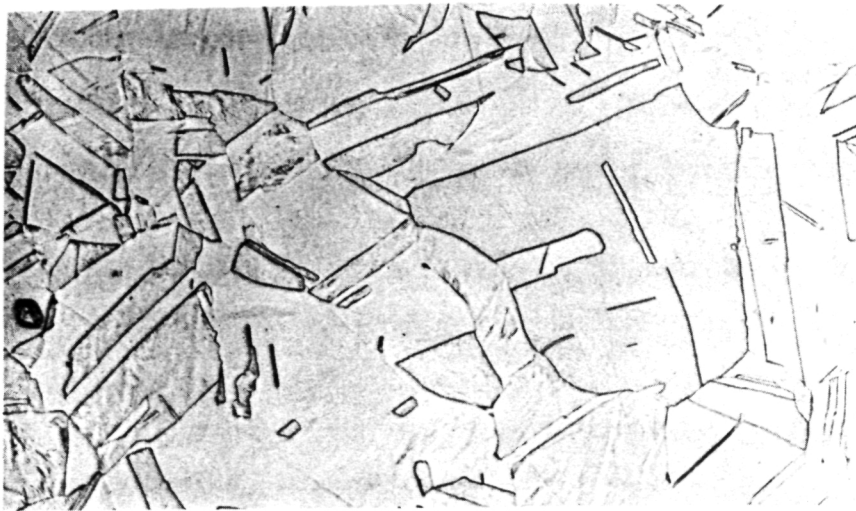
Mechanical properties testing indicated 0.2 percent offset yield stresses of 305.3 MPa for the AR condition and 277.7 MPa for the HTA condition, indicating that the HTA anneal actually had softened the material

---

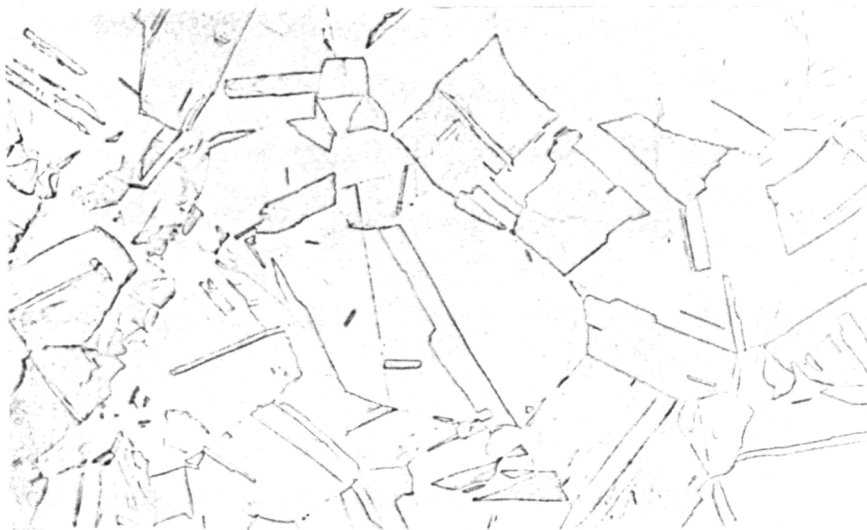
\*All heat treatment was done with samples sealed in pyrex vials evacuated and sealed in presence of 99.999 percent flowing Argon. Each vial contained a few grams of clean titanium chips to serve as a getter for any impurities.



(a) AR



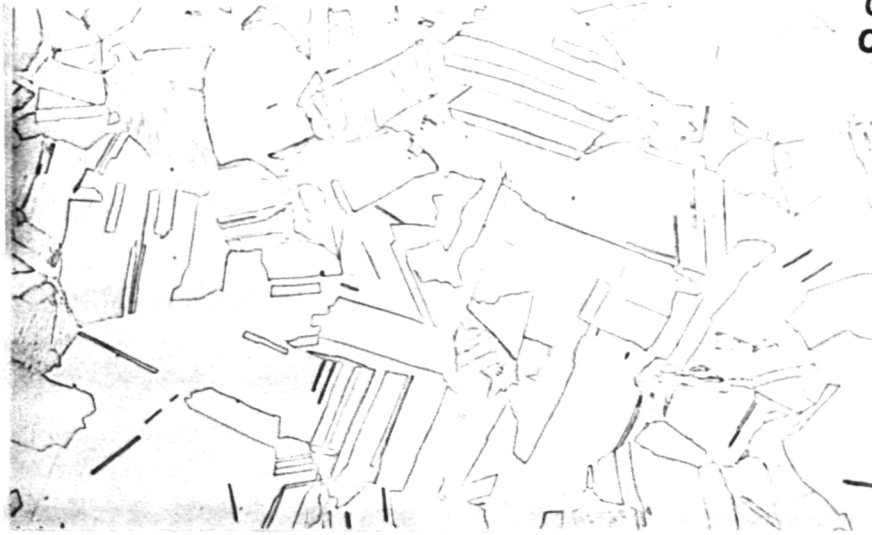
(b) AR1 - AR + 1 minute at 250 C



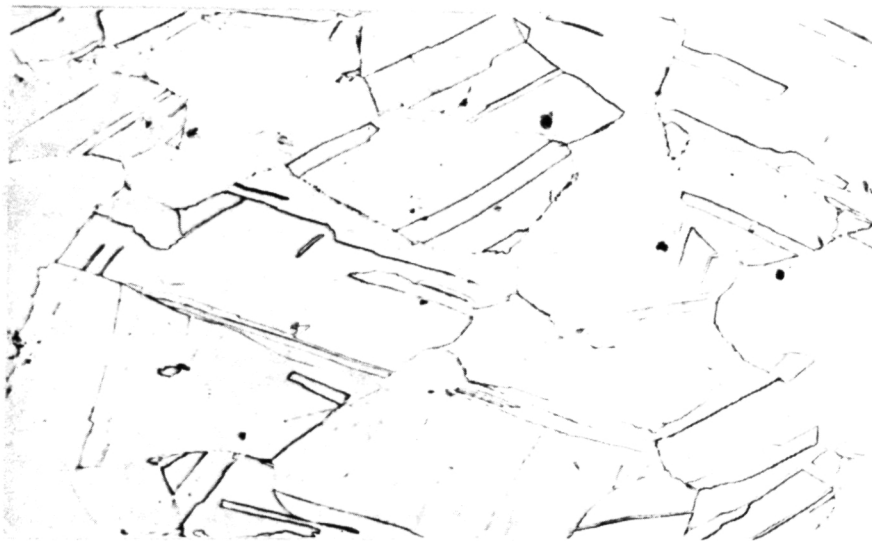
(c) AR1 - AR + 5 minutes at 250 C

FIGURE 8. MICROSTRUCTURES FOR VARIOUS HEAT TREATMENTS OF OFE COPPER (100X)

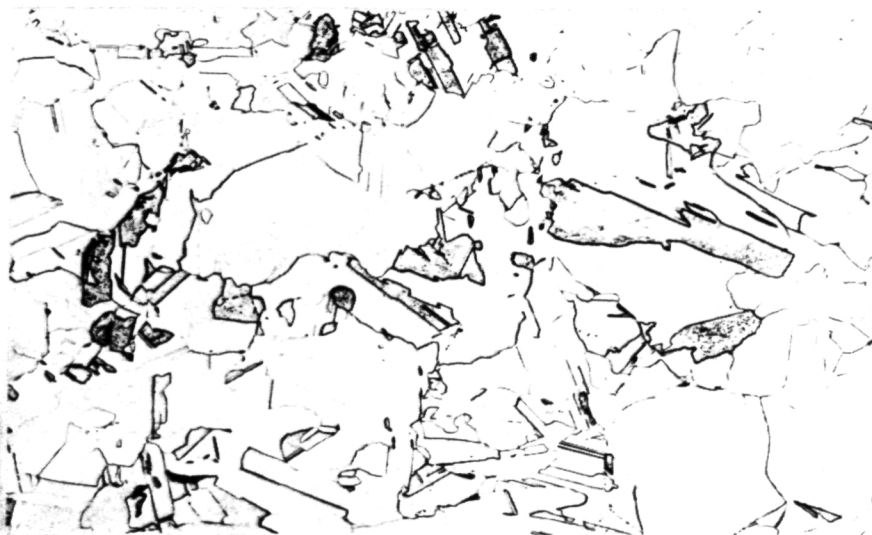
ORIGINAL PAGE IS  
OF POOR QUALITY



(d) AR10 - AR + 10 minutes at 250 C



(e) HTA - AR + 24 minutes at 250 C



(f) HTB - AR + 50 minutes at 270 C

somewhat. But this was not enough for present purposes. For this reason samples of the AR condition were annealed at 285 C for 50 minutes, an anneal hereafter termed HTB. Heat treatment B produced some recrystallization, as evident in Figure 8(f). The grain size was measured as ASTM  $2\frac{1}{2}$  to  $3\frac{1}{2}$  and included some finer grains as compared to the other structures, apparently due to the recrystallization. The hardness was 84.17 with a standard deviation of 16.96 (12 observations). The microstructural modifications produced a material with an 0.2 percent offset yield of 246.7 MPa, a value substantially lower than that for the AR and HTA materials.

### Damage Evolution and Crack Detection

Four methods were used to track the development of damage under strain control testing in this study. Stress response was measured continuously and served as a bulk indicator of microstructural changes and the difference in compliance due to cracking. Changes in the ultrasonic impedance, manifest as a mean shift in an analogue signal, also served as a bulk measure of damage. In addition, the ultrasonic impedance also served to define the formation and development of cracking, as evident in changes in the magnitude of reflected energy. Changes in surface topography, mapped via replication, served as localized measures of near surface microstructural changes, and also provided direct characterization of cracking. Lastly, changes in microhardness served as a measure of bulk microstructural changes.

### Stress Response

Results of studies directed at the evolution of damage under baseline histories in terms of bulk stress response are presented in Figure 9. The AR and HTA conditions produced cyclic softening. However, at lower strains HTB cyclically hardened while at large strains HTB cyclically softened. This hardening and softening was viewed as a macroscopic manifestation of microstructural reorganization prior to cracking (e.g., [37,38]). This involves a breakdown of the initial dislocation morphology into cells, at least for the range of strains studied herein [34]. Further discussion of the

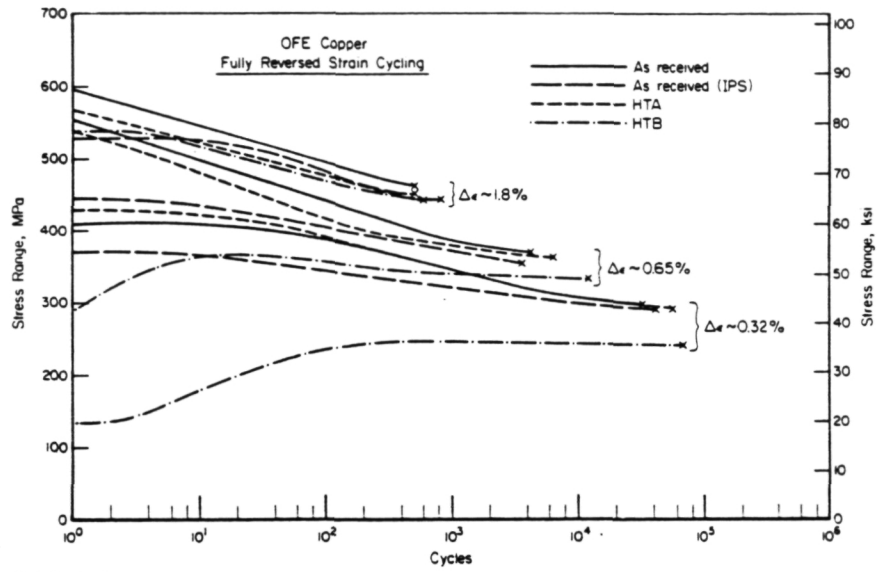


FIGURE 9. STRESS RESPONSE AS A FUNCTION OF CYCLES FOR THE OFE COPPER: AR, AR/IPS, HTA, AND HTB CONDITIONS

correlation between microstructural changes and changes in stress response follows later in the section titled Cyclic Deformation and Fatigue Behavior.

Stress response also served as a macroscopic indicator of the cracking process in that the specimen stiffness changed in the tensile direction with cracking, but remained more or less the same in compression once the crack faces close. This change was evident as an asymmetric decrease in tension load, as shown for example in Figure 2. If hardening or softening did not occur, and a single dominant crack formed, this asymmetric decrease in tensile stress response would define the net section area lost due to cracking. Provided that fractography permitted determination of the crack aspect ratio as a function of crack length, load drop also would define crack depth. Table 2 indicates that load drop\* provided a very sensitive indicator of the formation of small crack depths (under this set of conditions) for the segment configuration. However, for a semicircular crack configuration a one percent load drop equated with a quite large crack depth (650  $\mu\text{m}$ ). For the present study, macrofractography of failed specimens suggested that the initial aspect ratio was between 0.143 and 0.5, and that the depth of the crack was about twice that of the segment crack, as shown for example by the photomicrographs shown below the table. The cases shown illustrate double segment cracks for which a one percent load drop equated to a crack about 310  $\mu\text{m}$  deep.

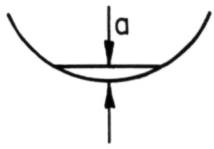
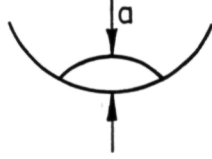

Crack depths listed in Table 2 were upper bounds on the actual crack depth if multiple cracks formed. They were also upper bounds in materials which soften since such softening at the crack tip would accelerate the load drop. Conversely, in materials which harden and form a dominant crack, these crack depths may not be an upper bound in that hardening at the crack tip would tend to offset the load drop due to lost cross-section\*\*. Results developed in this study indicated that the number of cycles associated with a 1 percent load drop (or the formation of a crack on the order of 1 percent lost area or upper bound depth of 310  $\mu\text{m}$ \*), was very large compared to the

---

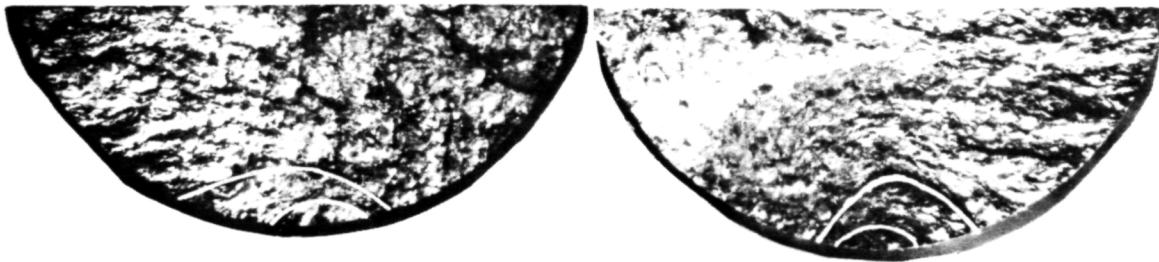
\*Load drop was assumed to be 1:1 related to crack area in the calculations presented in the table.

\*\*Engineering estimates indicated that hardening did not significantly offset the load drop due to cracking for the present study.

TABLE 2. AREA AND CRACK DEPTH AS A FUNCTION OF LOAD DROP

Load Drop, Percent	Crack Depth, a, mm					
	Crack Shape and Aspect Ratio, <sup>(a)</sup> a/2c					
	Segment		Double Segment		Semi Circular	
						
	0.101	0.164	0.072	0.155	0.5	} a/2c
1	0.310		0.192		0.65	} a
5		0.925		0.570	1.5	

(a) Crack shapes were mostly double segment with aspect ratios ranging from .14 up to about 0.5. Typical shapes such as that shown below indicated aspect ratios of about 0.3. Note that 2c is the distance along the surface while a is the crack depth.



number of cycles to grow that crack to separation. Furthermore, the load drop records indicated that the 1 percent load drop followed very soon after both the first discernable load drop and the life defined as initiation based on back extrapolated load drop (cf Figure 2). Note that these observations were contrary to the popular opinion that low cycle fatigue in ductile metals involves macrocrack propagation following almost immediate initiation of macrocracks. Whether or not this contrary observation was due to the material studied and the macroscopic nature of the definition of initiation is pursued in a few paragraphs.

### Ultrasonics

Ultrasonic tracking of damage evolution works on the principle that changes in the microstructure tend to alter the attenuation of sound waves as they pass through a material. This change in attenuation can be amplified and recorded in comparison to the initial (reference) condition. In turn this change can be correlated with physical manifestations of damage such as changes in hardness, surface topography, and stress response. Clearly, for this scheme to work the reference must remain invariant in time, and drift-free electronics must be available that match amplification needs. Furthermore, factors such as probe/substrate coupling must remain invariant with time, and be small compared to the amplified attenuation.

Calibration of the ultrasonic equipment indicated that the position of segment shaped electrical discharge machined (EDM) flaws 1 percent of the cross-sectional area (310  $\mu\text{m}$  deep)\* could be consistently located within the gage length. Thus the threshold for detection via ultrasonics as implemented in this study was a reflecting area on the order of one percent of the net cross sectional area. Studies with multiple flawed EDM samples indicated, as expected, that multiple small flaws on the same crack plane or in each others sound shadow tended to make signal interpretation difficult. These studies suggested that indications of cracking tended to provide upper bound estimates

---

\*Smaller depths were detectable, but not consistently.



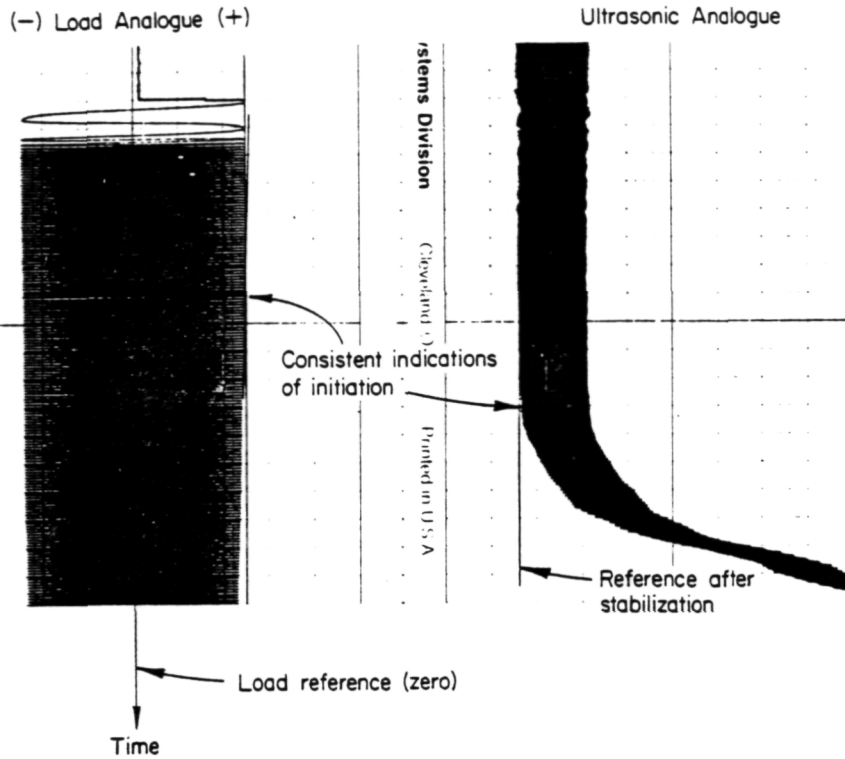
of the life to form cracks of the threshold size, whose sound reflective character was comparable to that of EDM flaws. Comparison of responses from actual cracks on the order of the threshold area suggested that for the OFE copper studied EDM flaws and cracks were indeed similar reflectors. Calibration of the ultrasonic analogue output with EDM flaw area indicated a correspondence could be developed with actual cracks. However, difficulties with the probe-specimen coupling introduced due to mechanical effects during test start-up/shut-down for purposes of making replicas caused the reference zero to shift. For this reason ultrasonic results were useful only as an indicator of cracking once the threshold crack area was developed.

Data developed indicated attenuation occurred during the period of transient hardening or softening. Thereafter changes were more subtle until indications of cracking were noted. Cracking produced analogue indications comparable to the attenuation observed during the transient period. However, the load dependent length of the specimen caused a cycle dependent variation to be superimposed on the attenuated response. The amplitude of this variation tended to increase with the increase in specimen length that developed with cracking. Generally, asymmetric load drop as defined in Figure 2 indicated initiation before the ultrasonic technique. Examples of this are apparent in the two typical strip chart recordings shown in Figure 10. Note that differences existed between the cycle identified as "initiation" using these methods of tracking damage. But, this difference was not of much consequence in a relative sense when compared with the number of cycles involved. The data developed indicated that lives defined as initiation by the load drop and ultrasonic schemes were equal within 1 percent, with only one exception.

### Surface Topography

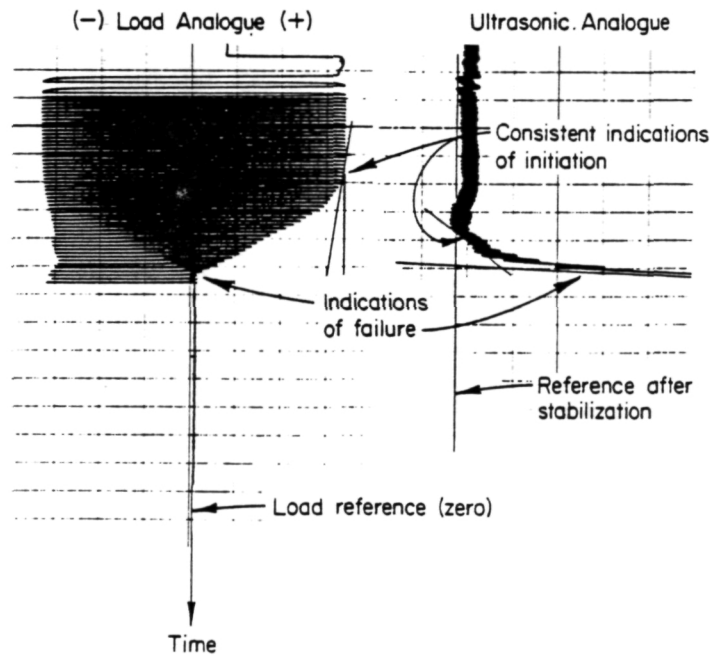
Single stage replication provided a more direct but also more tedious and expensive method of tracking damage as compared to stress response and ultrasonic measures. Acetate replicas were made at various stages of the life for every sample tested. Sufficient replicas were made to characterize the reference as machined/polished surface, and the surface after each major straining sequence, as well as at tenth points of the expected life. Funding

Test is stopped for replication and then restarted



(a) Specimen 16,  $N_f = 12,445$  cycles at  $\Delta e_2$  in HTB

Test is stopped for replication and then restarted



(b) Specimen 17,  $N_f = 853$  cycles at  $\Delta e_1$  in HTB

FIGURE 10. EXAMPLES OF ULTRASONIC RECORDS AND LOAD TRACES AS INDICATORS OF INITIATION

limitations precluded gold coating and detailed examination of all replicas for all specimens. For this reason results have been developed to characterize general trends and establish the relative effects of strain range, material condition, mechanical hardening and initial overstraining. Study of the seven specimens noted in Table 3 provided some insight into the effects of surface topography.

TABLE 3. SURFACE TOPOGRAPHY STUDY

Specimen	Condition	Strain History
35	AR	CA @ $\Delta e_1$
14	AR	CA @ $\Delta e_2$
4	AR	IPS followed by CA $\Delta e_1$
36	AR	IPS followed by CA $\Delta e_3$
29	HTA	CA @ $\Delta e_3$ started in compression
15	HTB	CA @ $\Delta e_3$
24	HTB	IOS for 100 cycles, followed by a DPS, followed by CA @ $\Delta e_3$

Results developed from the examination of surface topography for these seven samples are presented in Figure 11, parts (a) through (g). Each figure includes photographs at low (50X) magnification and selected photographs at one of 250, 1,000 or 5,000X magnification\* as needed to characterize the topography and illustrate trends. In studying these photographs, bear in mind that photographs of single stage replicas depict a negative impression of the surface.

A few general observations are in order before results are discussed on a specimen to specimen basis. At high strains the surface topography was rather uniform and began to develop early in the life. Continued cycling intensified surface features which tended to be aligned with the macroshear orientations for the specimen. The formation of what appeared to be long and

\*The study was made using the magnifications noted. However, to facilitate reporting, these magnifications have been reduced by about 0.5, resulting in magnifications reported in Figure 11 as 25X, 125X, 500X, and 2500X. As well some detail is lost using the reproduction procedure employed.

shallow Mode II cracks developed early in the life. Eventually Mode I cracks grew from areas containing Mode II/Mode I cracks, which evolved earlier from the long shallow shear oriented (Mode II) surface cracks. Lower intensities of cyclic strain led to trends comparable to those at higher strains, except the deformation was not homogeneous and consequently resulted in a reduction in the extent of surface area involved in Mode II cracking. This in turn produced fewer regions from which Mode I cracks could evolve. Initially softer copper exhibited more extensive and well developed Mode II cracking compared to its harder counterparts at equal cycle numbers or comparable life fractions. Initial prestrains served to create Mode II cracks earlier in the life. However, this topography was very limited in extent and intensity compared to that developed by continued cycling until the prestrain/overstrain history constituted a linear damage fraction of 0.4 to 0.5.

Study of all specimens indicated that the onset of Mode I cracking occurs very much later in life than did the formation of Mode II crack like features. Lives to form Mode I cracks correlated reasonably with the earlier discussed bulk measures of initiation. This suggested the popular view that the life of low cycle fatigue specimens made of ductile metals was spent in large part growing cracks, did not hold for the copper specimens examined. Furthermore, it suggested that load drop and other such bulk measures of "initiation" provided a reasonable characterization of the life to form Mode I microcracks,

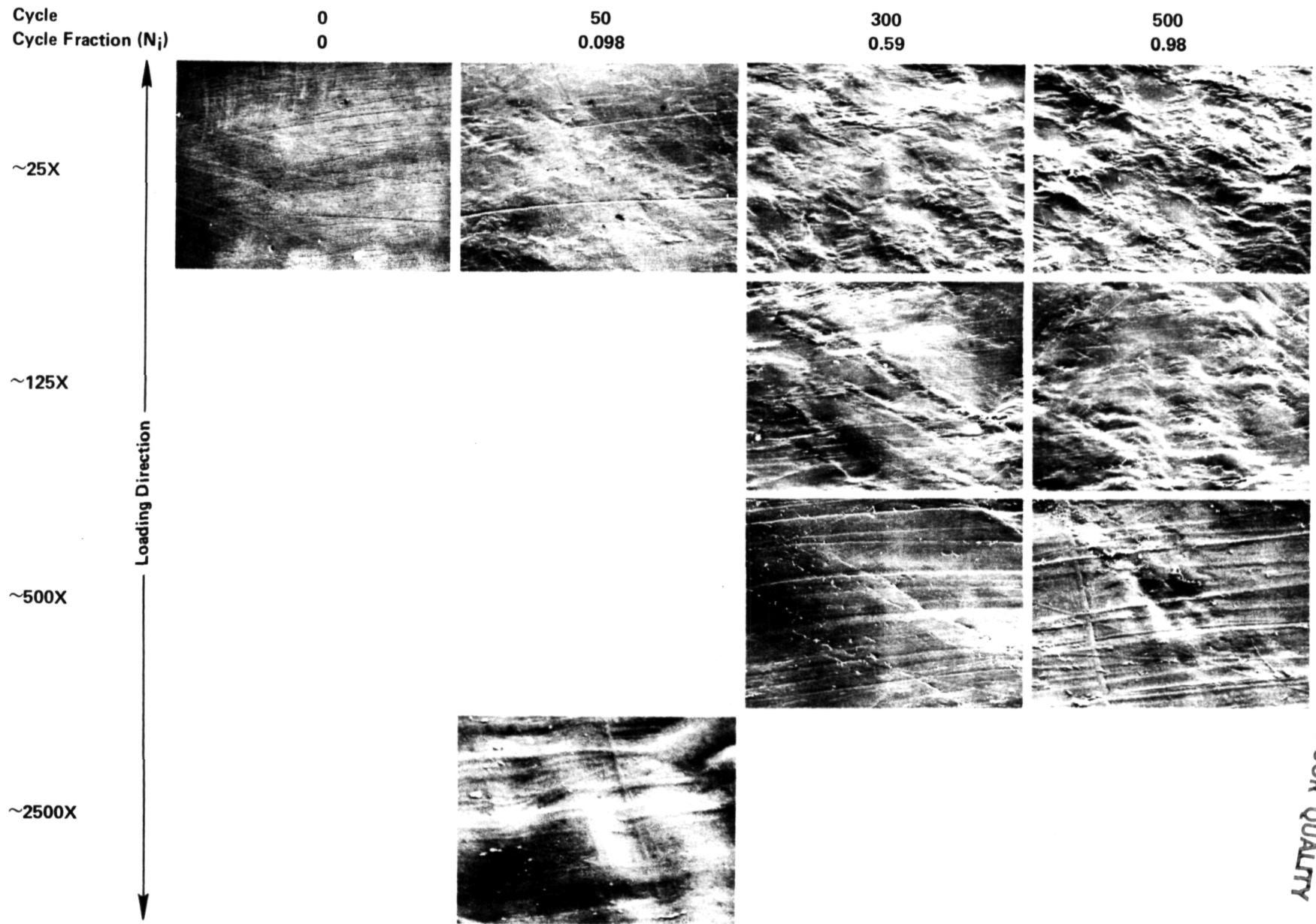
Whether or not the copper behaved differently from engineering alloys because it formed shear cracks in the absence of inclusions or second phase particles which may tend to directly form Mode I cracks in engineering alloys is open to speculation. Nevertheless, it was clear that long and shallow Mode II cracks which form early in the life were only of consequence when they became life-limiting. Mode II cracks became life threatening when they ceased to grow as shallow surface shear cracks by turning into combined Mode II/Mode I (perhaps as the Mode II crack grew into adjacent grains). Thereafter the Mode I component of the crack grew across the transverse net-section leading to failure. It was these Mode I cracks that most strongly reflected ultrasonic energy and resulted in the significant reduction in load used to define nucleation by back extrapolation (cf Figure 2).

Figure 11(a) presents results which show the evolution of surface topography in specimen number 35 tested under CA cycling at  $\Delta e_1$  in AR material. The reference surface showed some evidence of machining marks, but did not show evidence of preferential slip due to machining and polishing. After 50 cycles or  $0.1N_i$ , the surface began to show rumpling on axes inclined to the tensile loading direction. Slip traces were somewhat randomly oriented but tended to be aligned with the rumpling. The majority of the slip appeared to be oriented at or near the macroshear planes for the specimen. These same features were evident at 300 cycles or  $0.6 N_i$ , however, they were intensified, i.e., they occurred more frequently and were better developed. Slip traces perpendicular to the tensile axis were also evident as are Mode II crack like features. There was also a concentration of damage perpendicular to the tensile axis that developed within as well as across the checkerboard of shear oriented rumpling. This damage, which could lead to Mode I cracks, appeared to be best developed in regions of intense shear oriented rumpling. Some long and shallow intrusion like features were evident growing from these areas. Finally, results are shown at 500 cycles or  $0.98 N_i$  obtained near the site forming the fatal crack. A still more intensified development of rumpling and shear oriented cracking was evident along with pucker like features that formed in the heavily deformed regions. These pucker like features had a Mode II/Mode I character, as did many of the earlier pure Mode II features. Cracking appeared to occur by decohesion of damaged areas that had a Mode II/Mode I character, with the Mode I character evolving late in the life.

Results for cyclic conditions comparable to those for specimen 35, except for the introduction of the IPS, are shown in Figure 11(b) for specimen 4. Note that features of damage evolution and cracking present in part (b) compare closely with those in part (a). Discussion of these therefore will not be repeated. Given these similarities, the prestrain apparently had little relative effect on the surface topography. But this may be expected given the extensive flow that occurred with each cycle of  $\Delta e_1^*$  following the

---

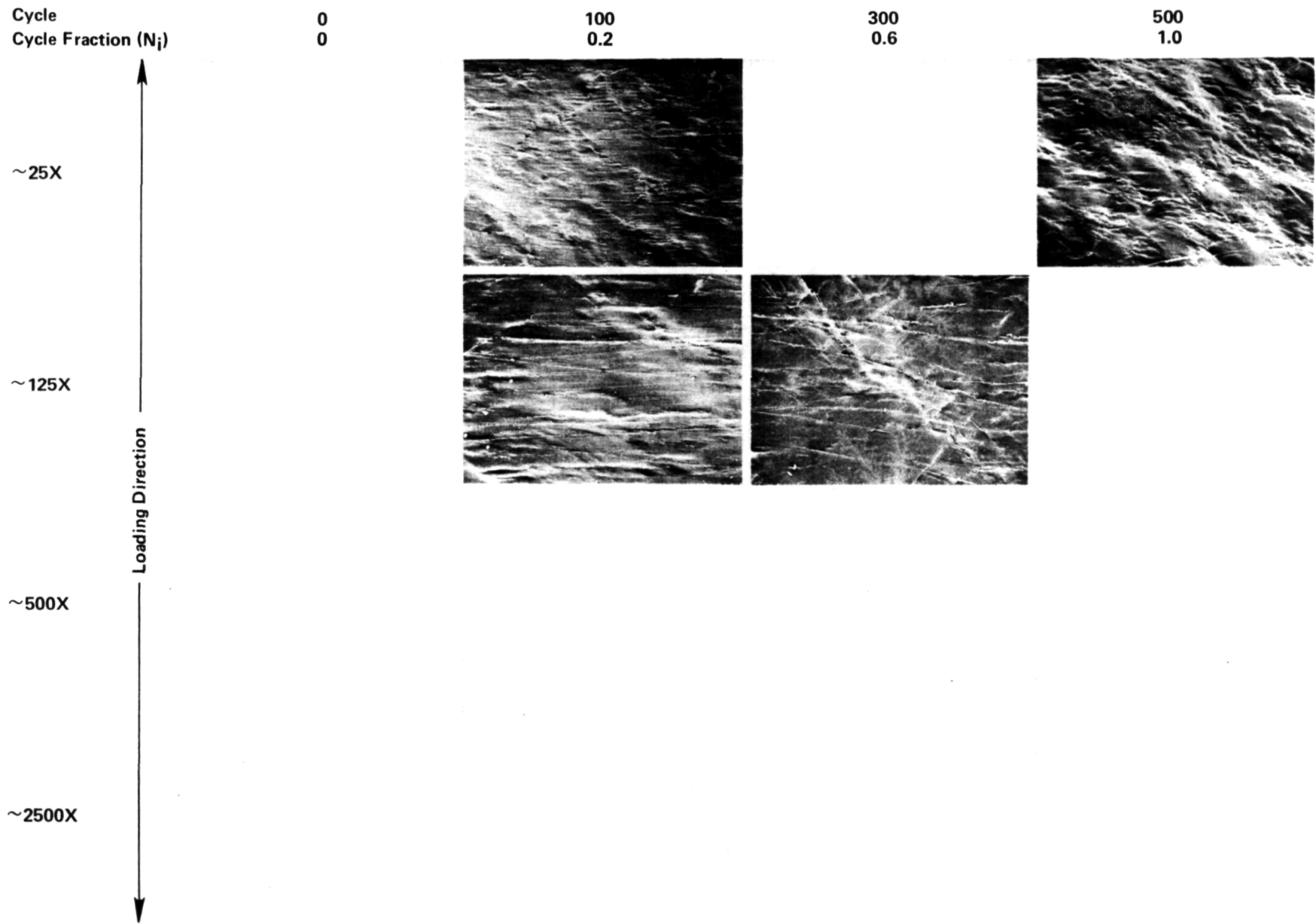
\*Study of the surface after the IPS at 5,000X indicated no change in surface topography had occurred, aside from formation of a few slip traces, as detailed next in discussing specimen 36. Thus the IPS altered the hardness mechanically without perceptibly influencing the surface topography.



ORIGINAL PAGE IS  
OF POOR  
QUALITY

(a) Specimen 35: CA at  $\Delta e_1$  in AR material;  $N_i = 508$ ,  $N_f = 572$

FIGURE 11. EVALUATION OF SURFACE TOPOGRAPHY IN OFE COPPER UNDER CYCLIC LOADING



(b) Specimen 4: CA at  $\Delta e_1$  in AR material following the IPS;  $N_i = 500$ ,  $N_f = 502$

FIGURE 11. (CONTINUED)



IPS. As with specimen 35, there was a gradual intensification in the topography as cycling continued. Note that the lives of specimens 4 and 35 were virtually identical, and in both cases a very few cycles of straining were required to grow (not nucleate) detectable microcracks (on the order of one percent of the specimen area) to their critical size.

Specimen 36 represents test conditions identical to those of specimen 4 except that the IPS was followed by a lower strain range ( $\Delta\epsilon_3$ ) in the case of specimen 36. Examination of the topography for this specimen, shown in Figure 11(c), indicated that features similar to those for the previous specimens developed. However, here the damage was very localized and was not as well developed. When crack like features were apparent they did not arise from the extensive network of shear flow evident at high strains. Such localization of damage and Mode II cracking was expected in that, as the strain range decreases, slip occurs selectively in grains where the crystallographic orientation favors slip. Cracking from well developed slip via decohesion was also expected to occur selectively in grains where the adjacent grains admit continued easy slip. Mode II cracking was again a precursor for Mode II/Mode I and Mode I cracking. Finally, Mode I cracking was again observed late in the life. Note that the results for 5,000 cycles indicate the surface topography was virtually identical to that of the virgin surface. In this respect the IPS did not alter the surface, but did mechanically change the bulk hardness. In turn this meant that topographic results for IPS and non IPS histories can be directly compared as though the IPS had not been imposed.

Consider now results for specimen 14, developed in AR material under CA cycling at  $\Delta\epsilon_2$ , shown in Figure 11(d). Observe that these conditions, which were bounded above by specimen 35 and below by specimen 36, developed a topography which was a cross between these bounds. At low cycle fractions the topography showed the very localized and light damage evident late in the life of specimen 36. However, by midlife this damage intensified somewhat developing evidence of the puckers and Mode II, and Mode II/Mode I, cracking reminiscent of specimen 35. The essential topographical features of specimens 36 and 35 were thus evident in specimen 14. The only major difference between these features as a function of  $\Delta\epsilon_1$ ,  $\Delta\epsilon_2$  and  $\Delta\epsilon_3$  was the intensity and



Cycle  
Cycle Fraction ( $N_i$ )

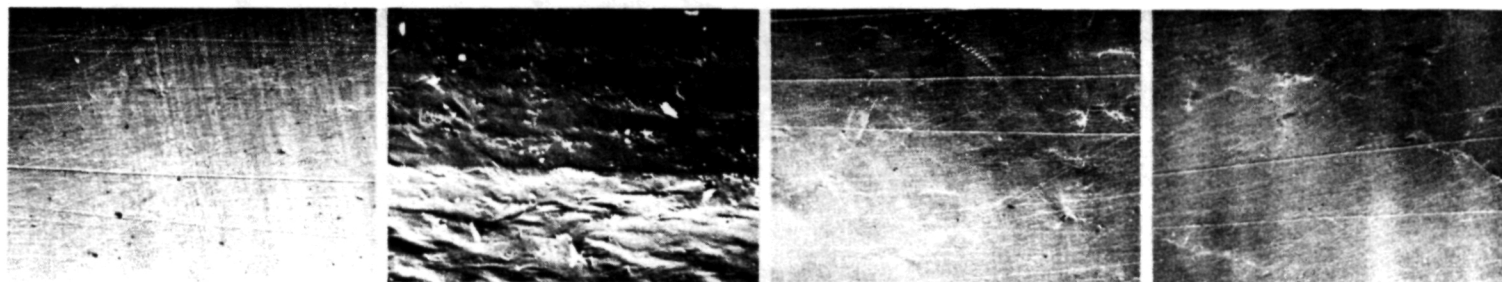
5,000  
0.082

10,000  
0.164

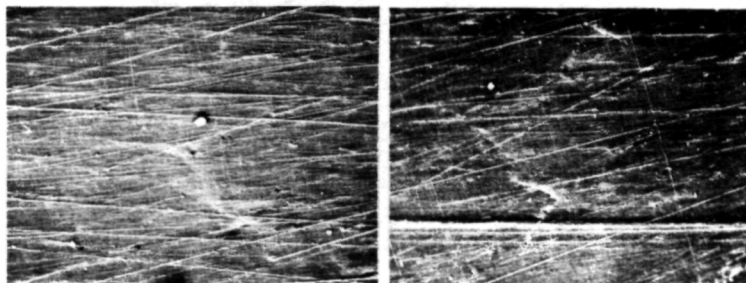
25,000  
0.61

40,000  
0.98

~25X



~125X



~500X

~2500X

Loading Direction

ORIGINAL PAGE IS  
OF POOR  
QUALITY

(c) Specimen 36: CA at  $\Delta e_3$  in AR material following the IPS;  $N_i = 41,000$ ,  $N_f = 44,878$

FIGURE 11. (CONTINUED)

Cycle  
Cycle Fraction ( $N_i$ )

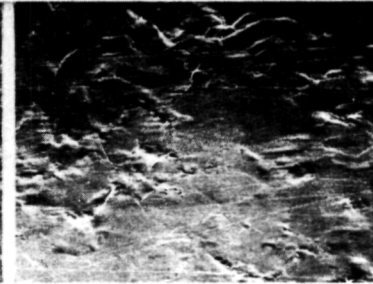
0  
0

500  
0.114

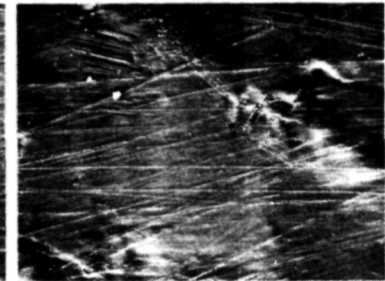
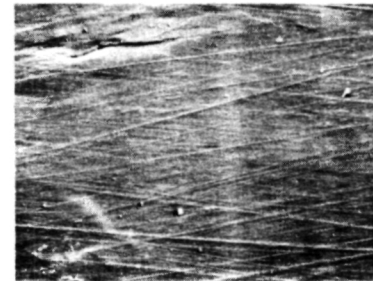
2000  
0.457

4500  
~1

~25X



~125X



~500X

↑  
Loading Direction  
↓

~2500X

ORIGINAL PAGE IS  
OF POOR QUALITY

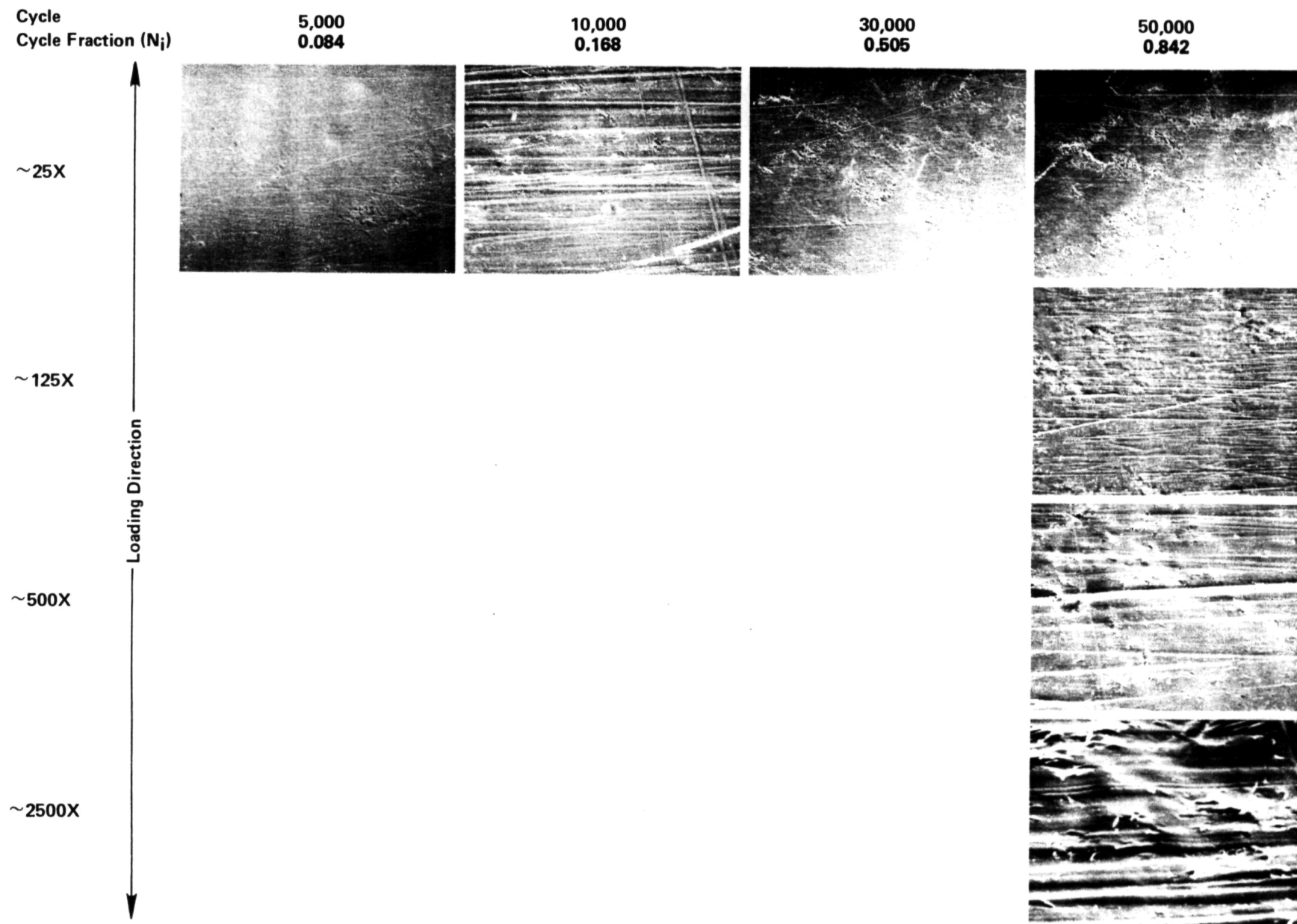
(d) Specimen 14: CA at  $\Delta e_2$  in AR material;  $N_i = 4376$ ,  $N_f = 5,836$

FIGURE 11. (CONTINUED)

distribution of damage. For all strain ranges the damage process was the same--after much shear mode cracking, life limiting Mode I cracks formed and grew across the transverse net section.

Differences in the initial hardness of the material were studied by comparing results for topographies characteristic of CA cycling at  $\Delta\epsilon_3$ . The AR condition is represented by specimen 36, shown earlier in Figure 11(c). The HTA and HTB conditions are represented by specimens 29 and 15, results for which are reported in Figures 11(e) and 11(f), respectively. Note in comparing these figures that the stages in life for a given cycle number represent increasing cycle fractions for the harder materials due to the increased fatigue resistance for HTB vs HTA vs AR conditions. These results showed the surface mottling to be initially sparse, but that it increased with further cycling. The mottling tended to be oriented along the macroshear planes, and developed earlier and more extensively in the softer materials. Toward the end of the life, puckers formed and Mode II/Mode I and Mode I cracking followed, just as had been previously discussed. Comparison of the topography indicated the damage became increasingly widespread and better developed as the material became more ductile, just as expected. Softer materials will have more grains favorably oriented for slip at a given strain range because, as reported earlier, their yield strength is reduced. Likewise flow within surface grains will be easier as compared to harder materials. In this respect, crystallographic notches at intrusions develop earlier in the softer materials and may serve to accelerate decohesion and initiation of all cracking modes. For this reason the life of softer materials may be limited at long lives by their earlier crystallographic notching as compared to their harder counterparts.

The effects of 100 cycles of IOS on damage topography are evident in the first of the results for specimen 24 shown in Figure 11(g). Note that the material studied was in the HTB condition. This softer material was expected to quickly develop extensive surface damage, particularly since the 100 cycles imposed represented a cycle fraction of about 0.143 ( $N_f$ ) under continued CA cycling at the IOS level. Such damage indeed developed with evidence of surface rumpling spread across the gage section. Examination up to 5,000X showed the presence of extensive shear oriented slip. But as expected given



(e) Specimen 29: CA at  $\Delta e_3$  in HTA material;  $N_i = 59,375$ ,  $N_f = 63,404$

FIGURE 11. (CONTINUED)

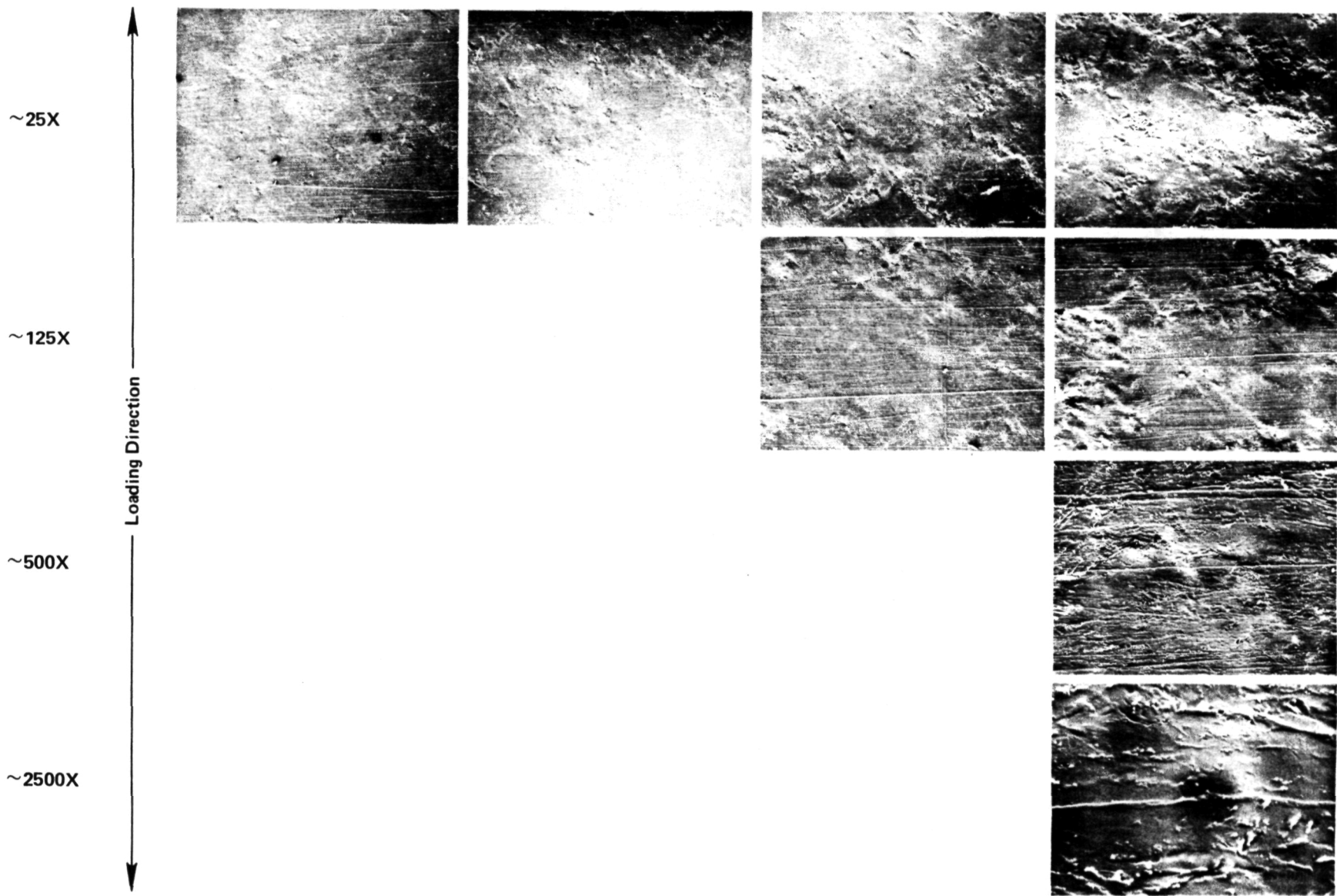
Cycle  
Cycle Fraction ( $N_i$ )

5,000  
0.075

10,000  
0.15

30,000  
0.449

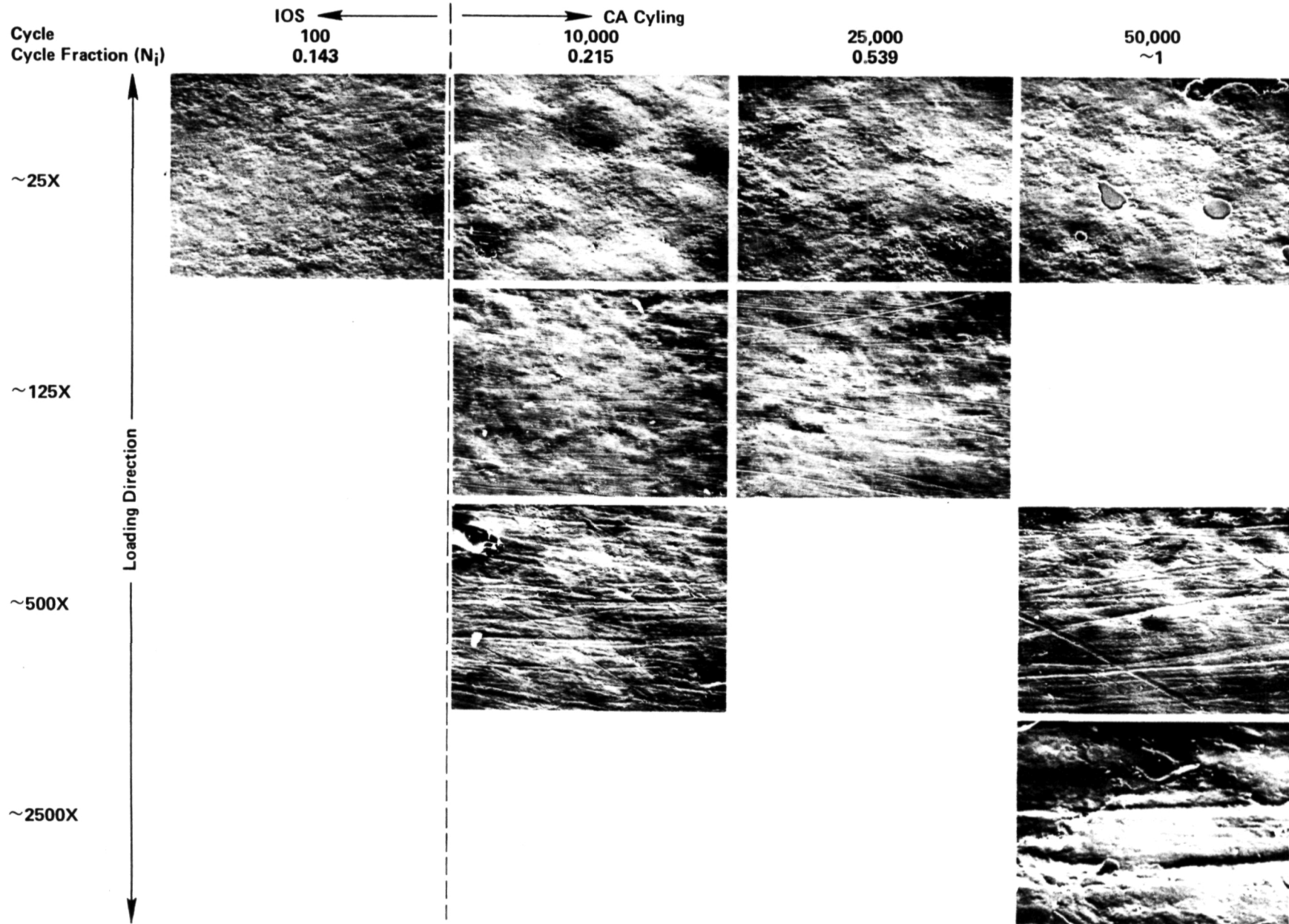
50,000  
0.748



ORIGINAL PAGE IS  
OF POOR QUALITY

(f) Specimen 15: CA at  $\Delta e_3$  in HTB material;  $N_i = 66,840$ ,  $N_f = 72,676$

FIGURE 11. (CONTINUED)



(g) Specimen 24: 100 cycles IOS followed by CA at  $\Delta\epsilon_3$ ;  $N_i = 46,428$ ,  $N_f = 52,625$

FIGURE 11. (CONTINUED)

the earlier noted gradual evolution of Mode II, then Mode II/Mode I, and finally Mode I cracking late in life, there was no evidence of cracking, or even puckering. With continued cycling at  $\Delta\epsilon_3$  following the IOS, the damage topography tended not to change in an obvious fashion\* until late in the life. When changes became apparent, there was evidence of puckering and Mode II/Mode I and Mode I cracking in areas adjacent to the site of the dominant crack.

Somewhat surprising was the fact that the IOS did not appear to significantly reduce the life as compared to pure CA cycling when the damage due to the IOS was linearly accounted for. In this case, the IOS reduced the life by about 12,700 cycles or 19 percent where an order of magnitude or greater life reductions are reported in the literature [5,39]. Whether or not this was due to differences in cracking processes between OFE copper and engineering alloys (Mode II to Mode II/Mode I to Mode I vs Mode I at inclusions and intermetallics, respectively) remains to be seen. Such considerations are deferred until all results are presented.

### Microhardness

Detailed microhardness surveys were made on the 12 specimens that characterized the baseline fatigue behavior of the HTB, HTA, AR, and AR plus IPS materials. Results for specimen groups 15, 16 and 17--26, 27 and 28--14, 21 and 35--and 4, 32, and 36, are listed in Table 4. Included in the table are mean values of the initial and final bulk hardnesses denoted as  $\bar{x}_0$  and  $\bar{x}_g$ . These hardness values were obtained by first sectioning and polishing failed specimens and then measuring the hardnesses in the gage section and at a low stressed location in the grip area. In most cases the results reported represent not less than six microhardness measurements. However, in some cases where scatter was large, more than 10 readings were made. Table 4 also lists the change in hardness, i.e., the difference between the initial and

---

\*Subtle changes like those observed for specimen 15 may have occurred but were not easily resolved because the surface rumpling tended to disguise such localized changes.

TABLE 4. CHANGE IN BULK MICROHARDNESS IN OFE COPPER UNDER CA CYCLING TO INITIATION

Specimen	History Strain Range	With IPS	Bulk Hardness (DPH)		Change in Hardness	
			Initial $\bar{x}_0 \pm \hat{\sigma}$	Final $\bar{x}_B \pm \hat{\sigma}$	Absolute (DPH) $\Delta \bar{x}_B = \bar{x}_B - \bar{x}_0$	Normalized $\Delta \bar{x}_B / \bar{x}_0$
35	$\Delta e_1$		108.7 $\pm$ 3	92.3 $\pm$ 7	-16.4	-0.151
	$\Delta e_1$	✓	106 $\pm$ 2	96.3 $\pm$ 10.2	-9.7	-0.092
	$\Delta e_2$		102 $\pm$ .6	78.3 $\pm$ .58	-23.7	-0.232
32	$\Delta e_2$	✓	99.3 $\pm$ 4.6	80 $\pm$ 3.5	-18.95	-0.191
	$\Delta e_3$	✓	93.7 $\pm$ 19.6	78.3 $\pm$ 4	-15.4	-0.164
21	$\Delta e_3$		96.7 $\pm$ 20	76.7 $\pm$ 9.02	-20.0	-0.207
26	$\Delta e_1$		104.8 $\pm$ 5.4	85.3 $\pm$ 5	-19.5	-0.186
27	$\Delta e_2$		105 $\pm$ 4.76	76.5 $\pm$ 1.5	-28.5	-0.271
	$\Delta e_3$		101 $\pm$ 1.4	84.5 $\pm$ 3.5	-16.5	-0.163
15	$\Delta e_3$		65.75 $\pm$ 8.22	72 $\pm$ 2.90	+6.25	+0.095
16	$\Delta e_2$		86.5 $\pm$ 12.8	87.5 $\pm$ 5.01	+1.0	+0.012
17	$\Delta e_1$		100.25 $\pm$ 4.5	82.17 $\pm$ 2.40	-18.08	-0.180



final mean bulk hardnesses. The change in hardness normalized by the initial hardness is also given in Table 4 for each specimen. In cases where the hardness increased these differences are noted as (+) whereas in cases where it decreased, the difference is noted as (-). Observe from the table that initially harder material showed negative changes while initially soft material showed positive changes at smaller strains and negative changes at larger strains.

### Cyclic Deformation and Fatigue Behavior

Under CA cycling the locii of the half life loop tips, shown in comparison to the monotonic responses in Figure 12, indicated each of the AR, HTA, and HTB conditions studied cyclically softens. However, this is an oversimplification in that hardening was observed initially followed by softening, and in one case pure hardening was observed, as evident earlier in Figure 9. The implications of this transient behavior will be pursued shortly.

Fatigue resistance data developed in this program are reported in Table 5. Included in the table are total, plastic, and elastic strain ranges  $\Delta e^t$ ,  $\Delta e^p$ , and  $\Delta e^e$ , stress range,  $\Delta s$ , cycles to initiation\*,  $N_i$ , and failure\*\*,  $N_f$ , and a description of the material heat treatment and strain history. Information extracted from the raw data of Table 5 or the mechanical response of the specimens is reported in Table 6. Included in this table are parameters such as  $s_{m\bar{x}}\Delta e^t$ , the ratio  $N_i/N_f$ , cumulative energy,  $\sum E_i$ , energy per cycle,  $E_i$ , cumulative plastic strain,  $\sum \Delta e^p$ , the product  $s_{m\bar{x}}\sum e^p$  and the mean change in flow resistance based on bulk and microstructural measures,  $\Delta s/\Delta s_0$  and  $\Delta H_B/H_0$ .

As the data in Tables 5 and 6 are used to further explore fundamental aspects of damage evolution and accumulation, and assess the viability of the postulate, these and other data will be introduced in graphical form. Recall that these data have been developed with a view to answering three earlier posed fundamental questions regarding the phenomenology of damage, for

---

\*Initiation was defined here by the back extrapolation technique defined earlier, cf. Figure 2.

\*\*Failure was defined here as separation of the specimen into two pieces.

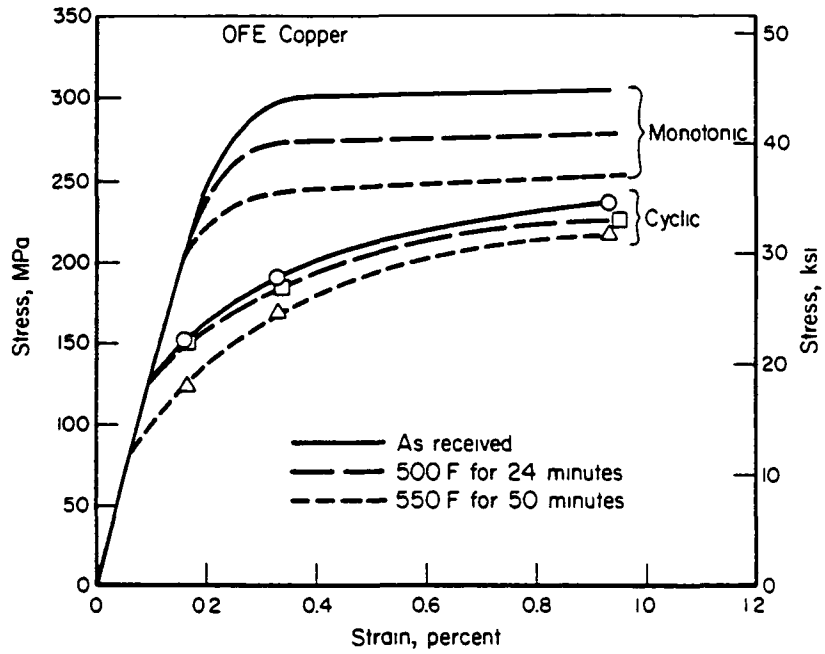


FIGURE 12. COMPARISON OF MONOTONIC AND HALF LIFE STRESS RESPONSE FOR OFE COPPER FROM SELECTED TESTS: AR, HTA AND HTB CONDITIONS

TABLE 5. FATIGUE RESISTANCE DATA DEVELOPED FOLLOWING THE TEST PLAN OF TABLE 1

Specimen Number	Strain Range, %		Stress Range (a)		Life, (b) Cycles		Condition	History
	Total	Plastic	Ksi	MPa	Initiation	Separation		
BASELINE CONSTANT AMPLITUDE CYCLING								
35	1.86	1.51	69.2	476.8	508	572	AR	CA
14	0.656	0.371	55.6	383.1	4,376	5,836		
21	0.323	0.096	44.2	304.5	32,520	35,698		
26	1.86	1.52	66.3	456.8	624	672	HTA	CA
27	0.65	0.374	53.8	370.7	6,525	7,806		
28	0.33	0.104	44.1	303.8	55,162	64,654		
29	0.33	0.105	43.9	302.5	59,375	63,404	Started in Compression	
17	1.85	1.51	65.8	453.4	818	853	HTB	CA
16	0.65	0.397	49.4	340.4	12,000	12,445		
15	0.33	0.147	35.7	246.0	66,840	72,676		
INITIAL PRESTRAIN THEN CONSTANT AMPLITUDE CYCLING								
4	1.83	1.48	67.0	461.6	500	502	AR	IPS+CA
32	0.645	0.368	54.0	372.1	3,629	5,019		
36	0.311	0.089	43.2	297.6	41,000	44,878		
37	0.164	--	--	--	DNF	DNF		
37R	0.316	0.090	44.0	303.2	32,127	36,550		
12	0.33	0.097	45.4	312.8	35,762	53,500	CA: 300,000 cycles at $\Delta\epsilon_1=0.164$ followed by cycling at $\Delta\epsilon_3$ to failure. Compression to -0.38%, tension to -0.19% then IPS to $\Delta\epsilon_3$ + CA at $\Delta\epsilon_3$	
INITIAL OVERSTRAIN WITH DECREMENTAL PRESTRAIN THEN CONSTANT AMPLITUDE CYCLING								
7	0.335	0.118	42.4	292.1	41,122	46,090	AR	20 IOS+DPS+CA
19	0.335	0.114	43.0	296.3	50,550	52,777		
11	0.339	0.122	42.4	292.1	35,980	43,004		
18	0.336	0.142	37.9	273.5	64,290	113,000		
9	0.339	0.126	41.6	286.6	41,745	63,218	AR	100 IOS+DPS+CA
24	0.341	0.130	41.1	282.3	46,428	52,625		
INITIAL OVERSTRAIN WITH DECREMENTAL PRESTRAIN THEN HTB FOLLOWED WITH CONSTANT AMPLITUDE CYCLING								
20	0.338	0.111	44.3	305.2	45,880	49,427	AR	100 IOS+DPS+HTB+CA
25	0.338	0.127	41.2	283.9	74,600	96,400		
BLOCK CYCLING								
23	0.337/ 2.04	--	--	--	55,084	67,427	HTB	BC
22	2.04/ 0.337	--	--	--	73,260	80,658	HTB	BC

(a) Half life stress range is reported.  
 (b) Initiation is defined by the back extrapolation technique.

TABLE 6. PARAMETERS RELATED TO THE FATIGUE RESISTANCE  
DATA PRESENTED IN TABLE 5

Specimen Number	Ni/N <sub>f</sub>	s <sub>mx</sub> Δe <sup>t</sup> , MPa	Σ E <sub>i</sub> , KJoules	E <sub>i</sub> /cycle, Joules	Σe <sup>p</sup>	s <sub>mx</sub> Σe <sup>p</sup> , MPa	Δs/Δs <sub>0</sub>	$\overline{\Delta H_B} / H_0$
35	0.89	4.43	3.51	6.91	7.75	1849	-0.286	-0.14
14	0.75	1.25	4.75	1.08	16.30	3126	-0.462	-0.23
21	0.91	0.49	5.05	0.16	34.07	5192	-0.366	-0.20
26	0.93	4.24	3.68	5.90	9.47	2167	-0.26	-0.185
27	0.84	1.21	7.11	1.09	24.75	4595	-0.46	-0.271
28	0.85	0.50	11.93	0.22	60.81	9253	-0.44	-0.163
29	0.94	0.50	--	--	57.07	8642	--	--
17	0.96	4.20	4.67	5.71	12.33	2798	0.135	-0.18
16	0.97	1.11	11.25	0.94	44.00	7500	-0.195	+0.012
15	0.92	0.41	15.00	0.22	89.75	11054	+0.428	+0.095
4	~1.0	4.22	3.04	6.08	7.61	1760	-0.281	-0.09
32	0.72	1.20	3.85	1.06	13.17	2453	-0.466	-0.19
36	0.12	0.46	5.46	0.13	40.70	6065	-0.347	-0.16
37	--	0.18	--	--	--	--	--	--
37R	0.88	0.48	--	--	--	--	--	--
12	0.67	0.52	--	--	--	--	--	--
7	0.89	0.51	9.02	0.22	44.90	6568	--	--
19	0.96	0.52	--	--	--	--	--	--
11	0.84	0.50	8.13	0.23	40.30	5895	--	--
18	0.57	0.44	13.61	0.21	77.30	10107	--	--
9	0.66	0.49	8.94	0.21	45.80	6573	--	--
24	0.88	0.48	10.22	0.22	52.40	7430	--	--
20	0.93	0.52	--	--	--	--	--	--
25	0.77	0.48	--	--	--	--	--	--
23	0.82	--	--	--	53.30	--	--	--
22	0.91	--	--	--	78.20	--	--	--

OFE copper over a limited range of lives. If the expected behavior was not observed or the results were inconsistent with the expected trends it would be concluded that the postulate was not viable. On the other hand, if the results were consistent with the expected trends and predicted behavior, it would be concluded that the postulate was viable. The approach to implement the study focussed on whether or not (1) hardness/ductility, (2) surface residual stress, and (3) surface topography developed in a characterizable fashion as a function of history. Further the approach involved exploring the history dependence of the material's fatigue resistance.

### Surface Topography

To this point it has been shown in some detail that the surface damage process was similar in all material conditions studied. These same results suggest that cracking at crystallographic notches due to well developed Mode II/Mode I microcracking would serve to limit life due to IOS or IPS under certain conditions. Results indicated that this effect would be particularly marked at longer lives and lower strains thus requiring a nonlinear damage assessment using a reference resistance curve that was a function of the strain history. Furthermore, the data clearly showed that there was a threshold damage state that must be developed before IPS or IOS would have a significant impact. Since this threshold evolves as a result of inelastic action, it is reasonable to speculate that this damage threshold will correlate uniquely with  $\sum \Delta \epsilon^p$  or  $s_{mx} \sum \Delta \epsilon^p$ . Available data indeed indicated a correlation was possible using such parameters, but the sparse data did not permit quantitative evaluation at this time. Thus it remains to explore hardness and surface residuals, and further demonstrate the history dependence of the resistance curve.

Correlation between surface topography and stress-strain history was explored by tracking the surface via replication under the action of various histories. Generally speaking, surface replication results indicated surface roughening continued throughout the life to initiation. The effect of initial prestrains was to roughen the surface creating a network of slip bands oriented at 45 degrees to the tensile axis (shear oriented). Initially soft OFE

copper samples exhibited a greater roughening than did samples of initially hard (drawn) OFE copper. The initial roughness developed, however, was very limited compared to that developed by continued cycling until the initial prestrain constituted a block of cycles with a damage fraction of about 0.4 to 0.5. In this respect the effect of initial prestrain certainly was seen to roughen the surface although the extent was small compared to the character of the surface developed at saturation. When prestrained lives (specimens 7, 9, 11, 18, 19, 20, 24, 25 in Table 5) were compared to non prestrained lives (specimens 15, 21 in Table 5), very little difference was observed except in cases where the prestrain constituted a significant damage fraction. As emphasized earlier, this trend was not expected given the apparent degrading effects of prestrains published for other materials (e.g.[5,36]). However this behavior was not inconsistent with the postulate, and indeed was easily rationalized in terms of a history dependent fatigue resistance curve, as demonstrated in a subsequent section.

### Surface Stress States

In this study surface stress state effects have been examined in terms of the life obtained under selected sequences over a range of strains. The possible effects of surface stress states have been studied here by starting tests in opposing directions - one in tension and one in compression. Because bulk inelastic action at higher strains typical of the OFE copper being studied lead to a homogeneous deformation state that washed out any microresiduals, consideration of this possible effect was limited to  $\Delta\epsilon_3$ . If there was an effect, this comparison would show that the test started in tension survived longer than its counterpart started in compression.

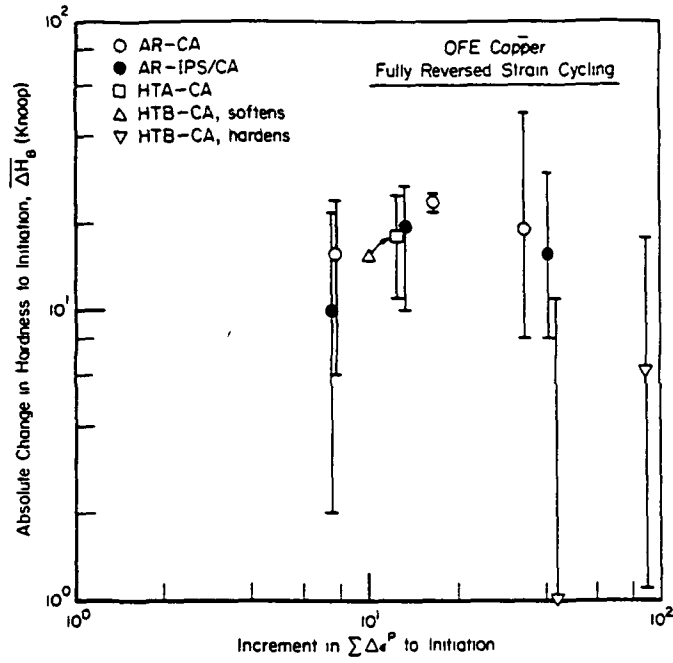
The results generated (specimens 28 and 29 of Table 5) showed virtually identical lives, differing by less than 2 percent at failure. In view of this limited comparison, it was tentatively concluded that surface stress state had nominally no influence on the damage process under the circumstances examined. This result was not surprising for the OFE copper which showed extensive plasticity, even at the lowest strain examined. It thus remains to be shown whether surface residual stresses develop or are of consequence at still lower strains in the OFE copper, or in engineering alloys.

### Measures of Damage

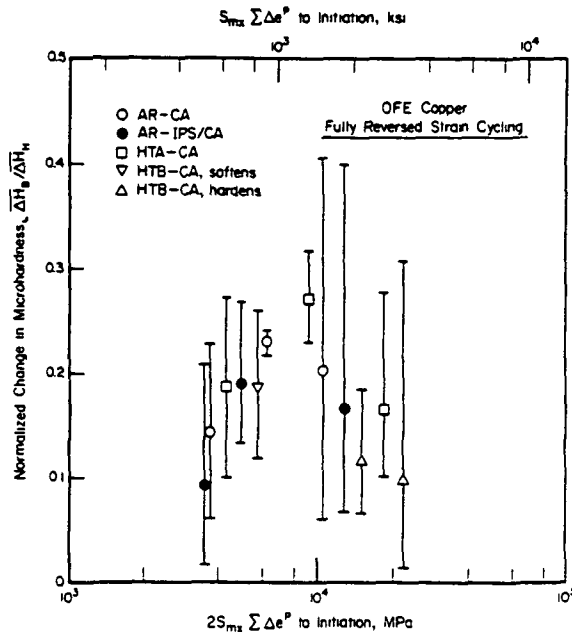
Consider now results developed to explore correlations of bulk and surface measures of damage with each other, and with other characteristic damage parameters. Tables 5 and 6 present data needed for this study. Observe from Figure 9 that the transient changes in stress response typically involved a period of initially stable to slightly hardening response followed by almost exponential softening. Higher strains and thus higher stable stresses tended to be associated with greater changes in stress whereas smaller changes occur at smaller strains since the driving force for transient action - plastic strain range - was reduced. In the context of cumulative plastic strain, this tendency was countered by the fact that at larger strain ranges less plastic strain accumulates before initiation whereas in the case of smaller strain ranges, the large number of cycles to initiation resulted in an extensive accumulation of plastic strain.

The net result of the counteracting factors controlling transient action is evident in Figures 13(a) and 13(b). In both figures changes in microhardness, postulated as being related to damage, first increase and then decrease. In this respect there were two distinct domains of response. Such a situation developed for OFE copper because of competing factors operative in all metals, as noted earlier. For this reason it may be anticipated to occur to some extent in all engineering alloys. It should be noted that the non-unique nature of this microstructural measure of damage does not preclude its being of value in a fundamental sense. This behavior is not inconsistent with the damage postulate, but it does lead to complications in tracking the damage process.

If changes in stress response are indeed measures of the microstructural process of damage, these changes in stress response should correlate with the just discussed changes in microhardness. As evident in Figure 13(c) the results introduced above do indeed correlate with changes in stress response reported in Table 6. Such a correlation suggests that bulk measures like stress response can indeed be used to characterize the microstructural changes leading to initiation, consistent with the postulate.



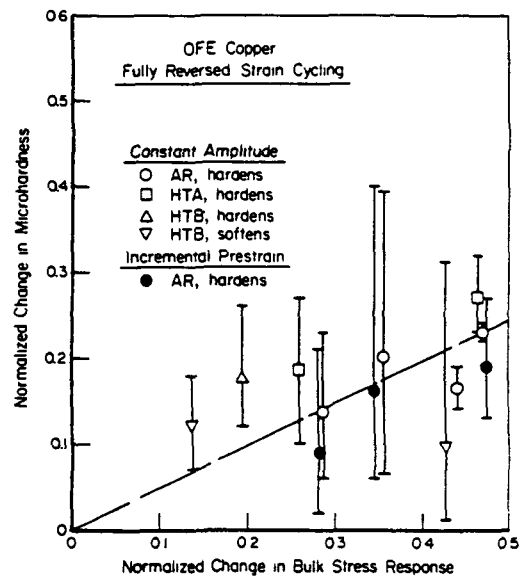
a. As a function of the increment in  $\sum \Delta \epsilon^p$  to initiation



b. As a function of  $2s_{mx} \sum \Delta \epsilon^p$  to initiation

FIGURE 13. TRENDS IN MICROSTRUCTURAL MEASURES OF TRANSIENT BEHAVIOR





c. As a function of changes in bulk stress

FIGURE 13. (Continued)

### History Dependence of the Fatigue Resistance

One key feature of the postulate arises with a view to answering the first of the earlier posed questions. "Should the reference data used in damage assessment reflect the history dependent hardness/ductility state of the material?" A related question is: can a test control condition such as  $\Delta e^t$  serve as a measure of the propensity for damage per cycle when the bulk stress, whose transient behavior is history dependent, does not vary in the same manner in both the reference data and the variable amplitude history being analyzed? The first question is of consequence to the postulate while the second addresses errors that may creep into damage analysis when a nonconstant damage per cycle is assumed to be constant.

The second question is more general and is addressed first. Data useful for this study may be taken for example from specimen 14 (Table 5). Analyses of the transient stress response (Figure 9) taken in conjunction with these data indicated that the dissipated energy per cycle was essentially constant for this test. In this sense dissipated energy per cycle reasonably matched the often made linear assumption that a given level of damage parameter produces the same amount of damage regardless of where it occurs in the history. In contrast, if  $\Delta e^t$  (or any purely strain or stress based measure) is used, the damage done in the first 0.25 percent of the life occurred at a level 38 percent above that in the last 2.5 percent of the life. During the first 2.5 percent, 12.5 percent, 37.5 percent, 62.5 percent and 87.5 percent of the life, the level of damage done compared to the last 2.5 percent of the life was, respectively, 23.4 percent, 10.5 percent, 4.97 percent, 3.13 percent, and 0.37 percent greater. The cumulative effect of ignoring this transient action amounted to a 2.13 percent error in the damage parameter, for the CA cycling imposed. For the AR material this translated into about 50 cycles to initiation at a life of about 1000 cycles - about 5 percent. In past, errors on this order have been accepted in exchange for the simplicity gained by ignoring the transient - thus steady state or half life values tend now to be the popular basis for developing reference data for damage analysis. However, greater errors may develop under BC histories and variable amplitude sequences as indicated in the following.

In situations such as that just examined, potential errors due to transient effects tended to be underestimated. For example, consider a history for which initial hardening increased the stress response, followed by CA cycling at a strain which did not promote softening. Calculations indicated that linear analysis based on total strain range as a damage parameter can underestimate the "effectiveness" of strain based damage as compared to that evaluated via a dissipated energy parameter by more than 60 percent, for the case of HTB material hardened and then cycled at a level on the order of  $\Delta\epsilon_3$ . This error arose because the hardening developed a stress level in excess of that developed in the CA test at the same strain range. This difference translated into an error in life of more than an order of magnitude, if CA cycling that did not cause softening followed the IPS that caused the hardening. In this respect, care must be taken to accommodate the shortcomings of the damage parameter. Note that the use of such a parameter essentially precludes successful implementation of the commonly used linear damage accumulation assumption, even before one starts damage analysis. It follows that complicated histories can produce a variety of counteracting transient effects that may influence life in a confounding fashion. Likewise materials which harden at high strains and soften at low strains can also produce confounding trends. Finally, note that softening would produce trends opposite to hardening.

In all of the just noted cases, the resistance curve used in damage analysis must be history dependent to account for the inadequacies of the damage parameter in regard to the assumption that each cycle causing a given value of that parameter does an equal amount of damage. The above discussion suggests that the result of violating this assumption will bias the error depending on the material and the history. Hardening materials can suffer more damage than expected, whereas softening materials may suffer less damage than expected using a pure strain based damage parameter. Histories which impose and sustain the effects of hardening or softening therefore are more discriminating than are those histories that tend to wash out the effects of the hardening or softening. These transient effects also are coupled with the possible influence of the larger cycles to significantly alter the evolution of the surface topography as compared to the CA case. This effect tends to

reduce the material's fatigue resistance, perhaps due to the early initiation of cracks which grow at higher rates and lower stresses as compared to the CA reference condition. Such coupling of transient effects and premature initiation is the situation commonly encountered in making damage (life) predictions for BC or variable amplitude (VA) cycling using CA reference data.

In view of the above discussion it appears that the fatigue resistance curve used in VA cycling or BC situations should be history dependent. (Clear evidence of this lies in the different resistance curves that develop in the absence of surface effects for AR material versus AR hardened by the IPS, results for which are shown in Table 5.) But, in view of the significance of this conclusion, the question merits further study herein for OFE copper - and still further study beyond this preliminary investigation for both OFE copper and engineering alloys. The next section begins with an examination of the common situation where transient effects and sequence induced premature initiation are combined through the use of  $\Delta e^t$  as a damage parameter. Thereafter transient effects are isolated from sequence induced premature initiation.

## EXAMINATION OF THE DAMAGE POSTULATE

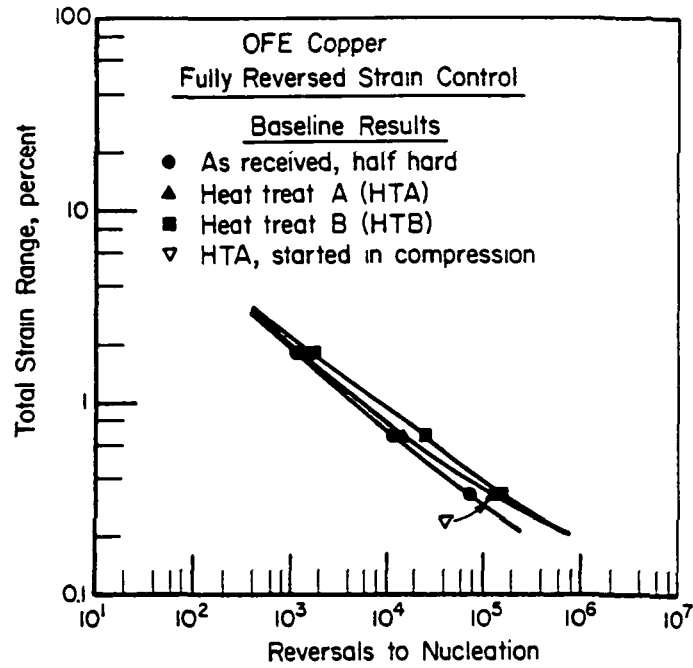
### History Dependence in a Strain Based Framework

Recall as indicated earlier that bulk changes in stress related to changes in microstructure which in turn related to damage. This meant that the material evolved in its hardness or ductility so long as microstructural changes evident in terms of changes in bulk parameters were occurring. Also, as just detailed it meant that if different stress levels develop for the same strain led to different values of the damage parameter in a given material, then differing amounts of damage per cycle develop even though the strain was the same. Consequently if different fatigue resistance curves can be developed for the same material in differing initial states of hardness/ductility one could conclude that a sample of material exhibiting transient response also exhibits differing fatigue resistances over its life. Because

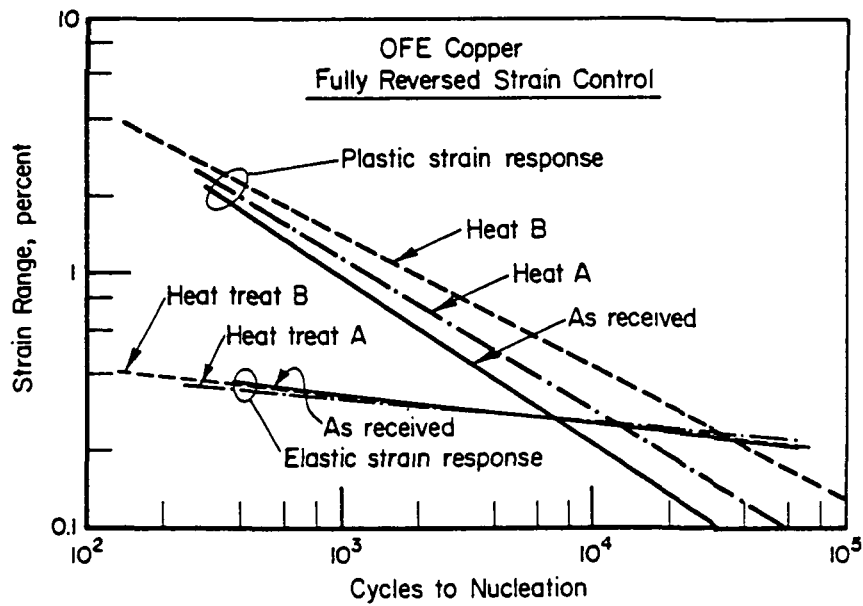
transient behavior is history dependent in general, one could conclude that the fatigue resistance is also history dependent, consistent with the postulate.

The possible history dependence of a material's fatigue resistance can be examined by comparing the fatigue resistances of a material in several different initial hardnesses/ductilities, based on the data in Table 5. These results represent OFE copper prepared in one of four hardnesses developed either by the IPS or by heat treating the half hard (drawn) material as detailed earlier. Testing was done at one of three identical strain levels -  $\Delta e_1$ ,  $\Delta e_2$ , and  $\Delta e_3$  - selected to cause nucleation at about  $10^3$ ,  $10^4$ , and  $10^5$  reversals. Raw data developed are presented in Figure 14(a). Observe that there is a layering of the data at high strains--longer lives being associated with increased ductility as expected. However, at the lowest strain this layering begins to wash out. This observation is less than surprising when interpreted within conventional wisdom which suggests curves for materials with different initial hardness crossover as life increases, in that long life is considered to be controlled by strength, not ductility. Regardless of why the layering begins to wash out, the data does layer indicating differing fatigue resistance curves for mechanically and thermally induced hardness changes such as develop under cyclic loading. This layering thus implies that different resistance curves exist at different stages of the life. This in turn implies a history dependence of the damage process consistent with the postulate. When coupled with the indications that transient effects cause a history dependence of damage as discussed previously, these trends are considered to constitute reasonable proof that the material's resistance curve under VA cycling is history dependent. Furthermore, unless transient effects can be accounted for by a damage parameter (which yields an equal increment of damage for a given level of damage parameter anywhere in the history up to nucleation), damage analysis will in general require a history dependent resistance. This last aspect is deferred for later consideration.

Another interpretation of the trends in layering also exists which is consistent with the postulate and these data, as well as the published data that lead to the conventional wisdom, as follows. Figure 14(b) presents the elastic and plastic components [20] of the results shown in part (a). Note



(a) Total strain-life behavior



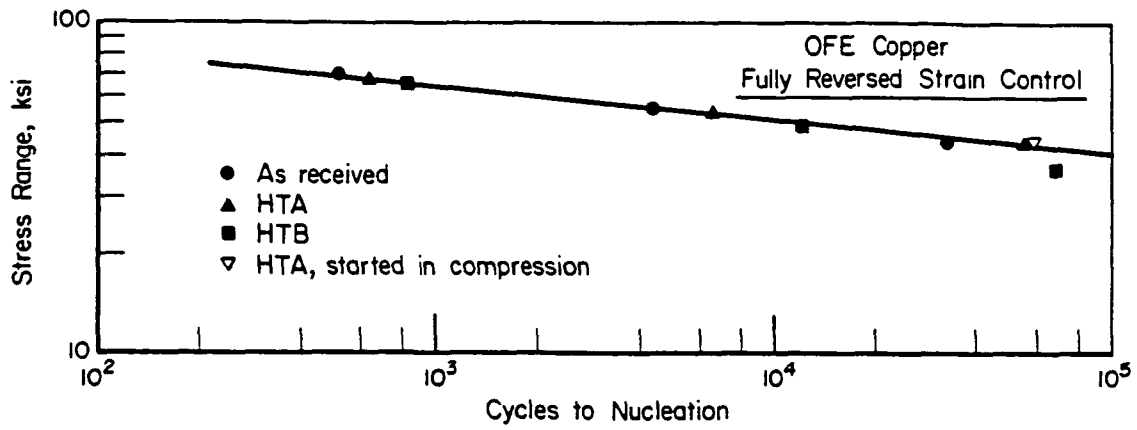
(b) Elastic and plastic strain-life behavior

FIGURE 14. FATIGUE RESISTANCE OF OFE COPPER AT 20°C IN FLOWING ARGON

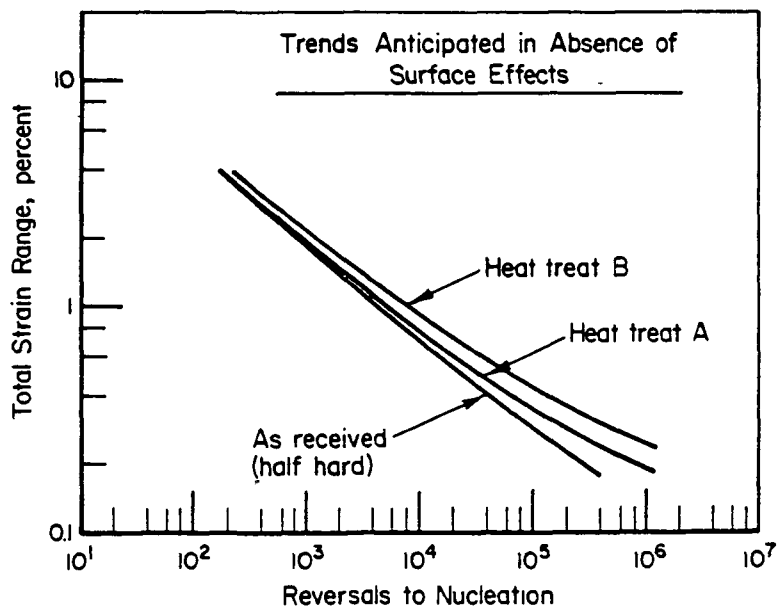
that the plastic components of the total strain layer as did the data based on the total strain. Note too that the stress response embodied in the elastic component is essentially independent of the initial hardness of the material. Figure 14(c) indicates this by a strong correlation of the stresses, with the exception of the one result for the softest material and longest life. Recall that Basquin's law [21] indicates the elastic strain (stress/E) life trend follows a power law out to the endurance limit. Extrapolating the elastic strain life line (excluding the just noted point for the time being) accordingly and adding that result to the plastic components in Figure 14(b) produces strain life trends which now layer at low strains as they do at high strains. The results of this construction are shown in Figure 14(d) with regard to the long life trend for HTB.

Clearly the construction of a small portion of Figure 14(d) is artificial and at odds with conventional wisdom that suggests these layered curves should cross. Note however that the constructed portion of the curve differs from conventional life data in that material resistance in the absence of surface effects is sought. Recall that the softest material has been noted earlier to develop a more intensified surface roughness more extensively than its harder counterparts, and that this process occurred much earlier in life. At shorter lives higher plasticity tends to wash out notch effects[19,40]. Also surface roughening tends to develop in all materials. At high strains the effects of surface are more or less equally present in the material conditions presented here, based on replication results. This means that at high strains the relative effect of surface tends not to be a factor while at lower strains it becomes important first for softer materials. The difference between the constructed portion of Figure 14(d) as compared to the raw data of Figures 14(a) and (b) therefore is postulated as being due to intervening surface effects. That is, it is suggested that instead of the fatigue resistance layering based on hardness/ductility throughout life, more ductile materials fail to achieve their potential resistance because intensified surface degradation intervenes by creating notches which serve to reduce fatigue resistance.

The interpretation of fatigue resistance as just detailed suggested that the so called "rocking chair effect" has a physical interpretation other



(c) Stress-life behavior



(d) Constructed total strain-life behavior



than balancing ductility for short life resistance against strength for long life resistance. Clearly strain-life data do exhibit this rocking chair effect, shown schematically in Figure 15. The postulate suggests these data trends develop as a consequence of layering bulk resistances based on hardness/ductility coupled with a loss of resistance at the surface by intervening notch enhanced initiation at longer lives.

In passing it is worth noting that the constant amplitude fatigue resistance at the lowest strain shown in the conventional plot (Figure 14(a)) is similar to that developed under various significant prestrains followed by cycling to failure at that strain level. This situation is at odds with other prestrain data which show a much reduced fatigue resistance attributed to the effect of the prestrain. However, if the plot of Figure 14(d) is used as the reference for constant amplitude cycling, the anticipated marked effect of prestrain is indicated. While this can't be taken as evidence supporting the postulate and the related reinterpretation of the rocking chair effect, it does indicate a further look at basic damage mechanics is warranted.

#### History Dependence in the Absence of Transient Effects

Consider now analysis of the history dependence of the resistance curve in terms of dissipated energy as a damage parameter. Note in this respect that the materials resistance is being correlated with dissipated energy--nothing fundamental is being assumed from which life is predicted from dissipated energy. The potential advantage of using dissipated energy as a damage parameter lies in its being nearly constant over life, as shown for the OFE copper in Figure 16.\* This tends to negate the influence of transients on the CA reference resistance curve, at least for the lives and material of interest in the present study. Following this scheme the value of the damage parameter per cycle is equal to the integrated dissipated energy divided by the number of cycles to initiation.

---

\*This nearly constant behavior is not typical (e.g. see [20]), nor is dissipated energy useful at long life where  $\Delta e^p \rightarrow 0$  as  $\Delta e^t$  decreases. Other parameters which circumvent these difficulties therefore should be sought.

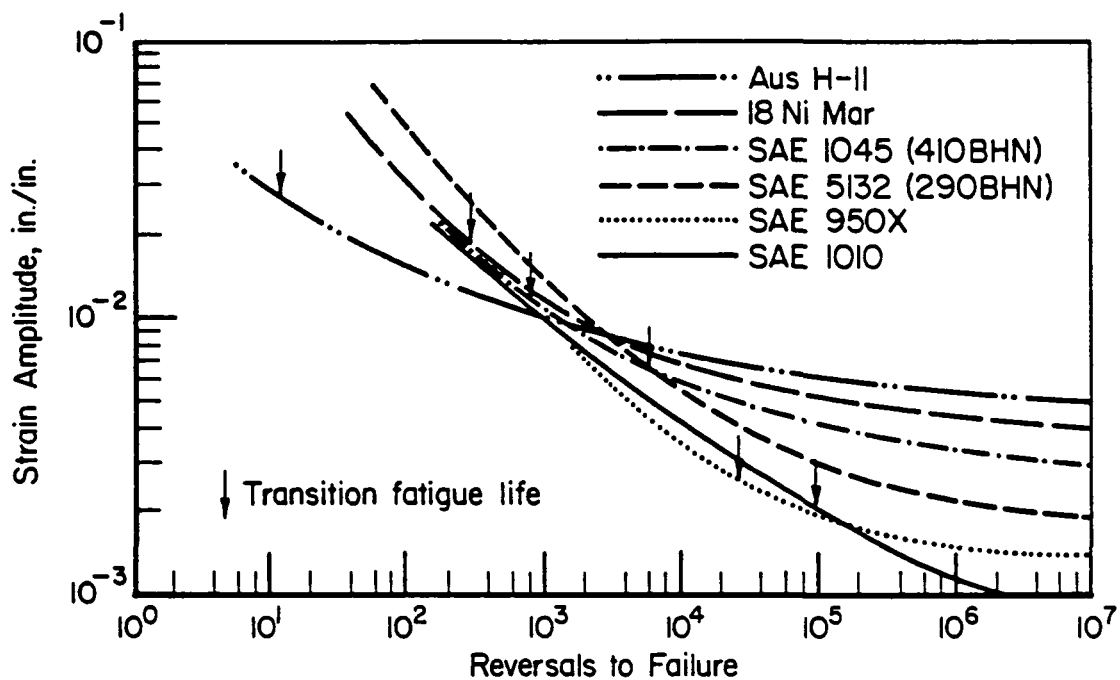


FIGURE 15. STRAIN-LIFE CURVES FOR A VARIETY OF STEELS:  
NOTE THE CROSSOVER TENDENCIES AND THE FACT  
THAT STRONG MATERIALS ARE BEST AT LONG LIVES  
WHILE DUCTILE MATERIALS ARE SUPERIOR AT SHORT  
LIVES (AFTER (41))

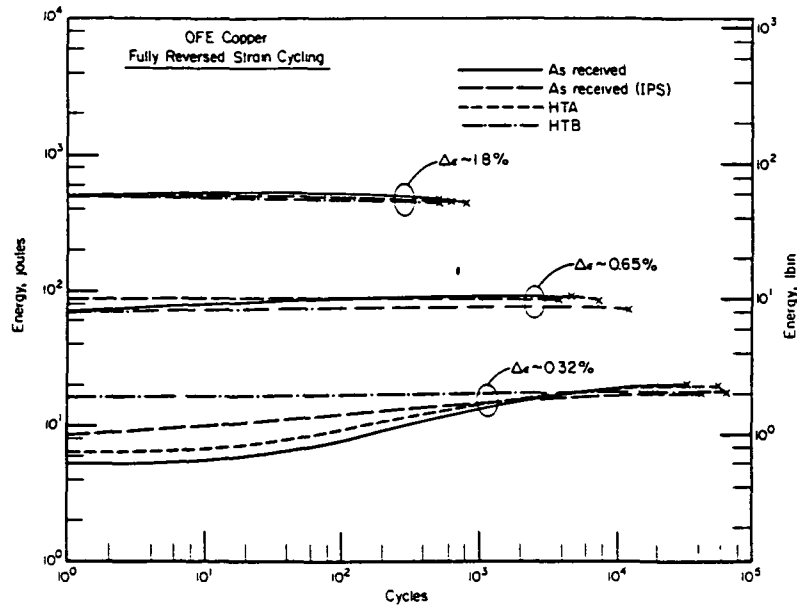


FIGURE 16. TRANSIENTS EVIDENT IN DISSIPATED ENERGY AS A FUNCTION OF CYCLES

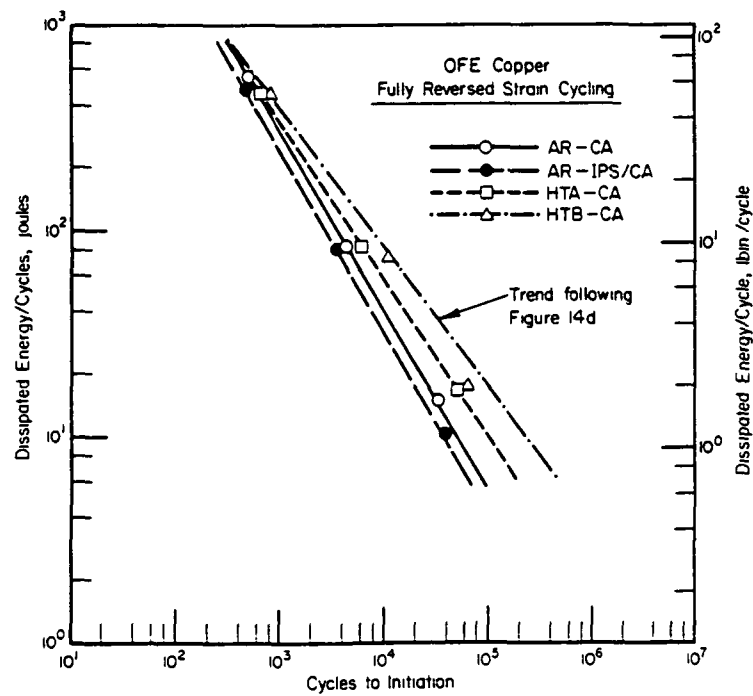


FIGURE 17. FATIGUE RESISTANCE AS A FUNCTION OF DISSIPATED ENERGY

Figure 17 plots dissipated energy versus cycles to initiation as just detailed, and it shows the same layering evident in Figure 14.\* Because transients occurring during the life have been negated in developing these histories such as IPS early in the life are thus expected to have a resistance curve shifted toward the left (decreased life). Indeed, although the difference is not too great, this is exactly the result observed for the AR material when the CA cycling is preceded by IPS.

As noted in dealing with the topography for the IPS, its effect is observed to be inconsequential for the AR material. For this reason, the entire shift to decreased resistance for the AR material must be ascribed to a reduction in the innate resistance to cracking of the bulk material. In this respect it is noted that the IPS cyclically hardens this material, and the following cycles do not cause softening to the level in CA tests of AR material. Given the trend of reduced life with increasing hardness (decreasing ductility) evident in Figures 14 and 17, the results for the IPS hardened OFE copper match exactly the trend predicted from the damage postulate. That is the fatigue resistance of the bulk material is controlled by hardness (ductility) changes due to the deformation history. It follows then (in the absence of history related differences in the surface topography) that differences in the bulk resistance of the material can be characterized in terms of the current hysteresis loop shape and deformation resistance normalized to some reference condition. The best material reference condition is one for which transient effects are minimal.

Conveniently, deformation resistance and loop shape vary in a unique history dependent fashion which can be characterized as functions of  $\int \Delta e P$ , with respect to some reference deformation condition - say that characterized by the monotonic stress-strain curve. Differences in fatigue resistance

---

\*Note that in this figure the long life behavior for HTB material has been developed following the construction used in Figure 14(d). Recall that this construction attempts to develop the fatigue resistance of the bulk material from the actual behavior which represents an increased bulk resistance offset by the well developed surface which acts as a distribution of notches to increase the surface strain above the bulk strain. In this sense, differences in the fatigue resistances of the material conditions shown in Figure 17 does not depend strongly on surface topography. Instead bulk properties control.

evident here are due solely to innate differences in the bulk resistance of these materials to crack initiation. According to the postulate, this is due to the history dependence of the deformation response. Soft material, such as HTB, harden under cyclic loading whereas hard material, such as AR/IOS, soften. Certainly these contrasting transients complicate the picture. But, fortunately for present purposes, such transients can be simply tracked and accurately predicted via computer models (e.g., see [5]). Consequently, this added degree of complexity does not adversely complicate damage analysis under variable amplitude (VA) cycling. However, it will enhance the accuracy by accounting for history dependent nonlinearities in damage assessment, while retaining the simple nonarbitrary assumption of linear accumulation.

It is interesting to explore the implications of the above suggestion that the bulk state of the material controls fatigue resistance in the absence of strongly different surface topographies. Consider first the results of specimens 7, 9, 11, and 19 subjected to various amounts of the IOS\* (20, 100, 50 and 20 cycles, respectively). Observe from Table 5 that the lives to initiation for these specimens do not show an ordered pattern in life reduction with increased number of cycles of IOS. The mean life for the group is 42,394 cycles with a standard deviation\*\* of 6046 cycles. All of these lives are in excess of the life to initiation observed for the non IOS material represented by specimen 21 (32520 cycles).

The fatigue resistances for IOS and non IOS specimens imply that the IOS (1) did not alter the surface to enhance initiation as compared to the non IOS case and (2) either the IOS increased the innate resistance to cracking of the bulk material, or reduced the effective driving force for damage, or induced beneficial surface residual stresses. Both (1) and the last item of (2) have been shown earlier not to be factors in this study. Regarding the driving force, the CA value of  $\Delta e$  is the same in all cases. However, the

---

\*Note that the IOS was followed by an IPS to wipe out any mean stress due to the stepdown in strains.

\*\*The significance of this number is questionable in a rigorous statistical sense - its use here is as a relative measure of scatter. Its usual statistical interpretation is not invoked.

magnitudes of the dissipated energies per cycle are higher in the case of the IOS plus CA, suggesting the lives for these histories should be shorter, but certainly not longer as was observed.

One possible explanation for this inversion of expected trends follows from the postulate: differing innate resistances to cracking develop due to the differing deformation histories imposed. Study of deformation responses shows the IOS data soften very rapidly to levels somewhat below their non IOS (CA) counterpart. Based on Figure 17, this means that the fatigue resistance curve for the IOS specimens actually lies to the right of AR material trend. This of course means longer lives for the IOS specimens, just as observed.

A test involving a slightly more complicated but less severe history as compared to the just discussed IOS cases was also performed, as indicated in Table 5 for specimen 12 made from AR material. This specimen was initially overstrained in compression and then partially unloaded so that a compressive mean strain remained. Following this the specimen was subjected to 8 cycles of incrementally decreasing amplitude to reach  $\Delta\epsilon_3$ . The slight compression mean stress was removed by a corresponding reduction in the mean strain. Following this, CA cycling at  $\Delta\epsilon_3$  was applied until failure occurred. The result after about 30 reversals of this CA history was a hysteresis loop bounded in energy content by specimens 21 and 36, but involved a somewhat increased stress for the same total strain range ( $\Delta\epsilon_3$ ) as compared to either specimen. The postulate indicates that the life of specimen 12 should be bounded above by the AR curve (specimen 21) and below by the curve for the AR material after the IPS (specimen 36), for the same level of damage. As can be found by study of Figure 17 at the damage level of interest, the life to initiation for specimen 12 was indeed so bounded. While this in itself does not prove the viability of the postulate it is yet another result qualitatively consistent with it.

The result for specimen 12, like most of the others, is not exactly what is expected based on trends in the literature. Yet it, as well as the other results discussed to date, qualitatively fit predictions of the postulate. Significantly the postulate can qualitatively explain the more typically observed literature trends as well - but further discussion of this is deferred until completing this section dealing with this investigation.

Results were also developed for IOS of HTB material using specimens 18 and 24. Specimen 18 had a 50 cycle IOS, while specimen 24 had a 100 cycle IOS history. For these specimens hardening was greatest in specimen 24, and the rate of softening following the IOS was slowest and occurred to the least extent in specimen 24 as compared to specimen 18. The postulate indicates that specimen 24 should not last as long as specimen 18 given the same damage level is imposed in that the innate bulk resistance of specimen 24 is less than that of specimen 18. Such a result indeed developed. Table 5 shows their lives are 64,290 and 46,428 cycles to initiation, respectively. However, Table 5 also shows that the damage levels imposed on specimens 18 and 24 actually differed. The energy per cycle introduced was greater for specimen 24 as compared to specimen 18 (17.33 joules vs 16.45 joules; see Table 6), even though the CA strain was the same. This difference in energy levels can be accounted for using the slope of the HTB data of Figure 17 to define the rate of change of resistance as a function of dissipated energy level. Normalized against specimen 18 with its observed life of 64,290 cycles at an energy level of 16.45 joules/cycle, the expected life of specimen 24 at 17.33 joules/cycle is in excess of 60,000 cycles in the absence of a deformation history dependent resistance curve. The observed life of 46,428 cycles therefore is reduced compared to specimen 18 at the same energy level as expected based on the postulate.

Note too that both IOS specimens 24 and 18 softened at a slower rate and to a lesser extent than the non IOS specimen (number 15 in Table 5). Therefore, according to the postulate, specimen 15 should survive longer than either specimen 24 or 18. Such was indeed observed, a result which again points to a dependence of the innate fatigue resistance of a material on the deformation history.

Consider now the IOS results developed for specimen 20, which started as AR but following the IOS was heat treated to the HTB condition. For this specimen the first 100 cycles did damage in the AR condition which, based on Figure 17, occurs at a just slightly faster rate than it would in the HTB condition. Following the IOS, the deformation history was wiped out by the HTB creating essentially virgin bulk material with some initial surface damage. Cycling of this specimen in the HTB condition produced a gradual

softening to a condition almost identical to specimen 24, but somewhat harder than the CA reference case (specimen 15). The postulate suggests that the life of specimen 20 should be reduced from that of specimen 15. Furthermore, given its deformation history is similar to that of specimen 24, comparable lives are expected. Interestingly, both qualitative predictions of the postulate are borne out in the lives observed, as evident in Tables 5 and 6.

Specimen 25, which starts as HTB but after the IOS is again subject to HTB, also constitutes an interesting qualitative test. The first 100 cycles in this test are identical to the first hundred cycles in specimen 15. After reheat treatment to HTB some of the prior mechanical history remains, as it did for specimen 25 because the deformation response upon reloading showed higher yield stresses than did AR material subjected to HTB. This difference means that specimen 20 gradually softens, just as specimen 25 did, except the rate of softening is somewhat slower and the extent somewhat greater in specimen 20 as compared to specimen 15. Qualitatively the harder specimen (number 20) is expected to fail before the HTB OFE copper reheat treated after further cold working (specimen 25). This further cold work enhances recrystallization and would develop a material that is softer (more ductile) than that for HTB. Given the trend of resistance with hardness evident in Figure 17, this material's fatigue resistance curve would lie to the right of that for HTB. This new trend is the upper bound to the life for specimen 25, because some life is exhausted by the first 100 cycles of IOS. Unfortunately in the absence of the reference curve for this double heat treated and cold worked material little can be said quantitatively. But the observed life of 74,600 cycles is well in excess of the life for specimen 15 (66,840 cycles).

It should be noted that concern must in general also be given to the effect of specimen surface topography that develops differently from the reference CA condition. The fact that the trends in Figures 14 and 17 lie well beyond the observed life for specimen 15 (HTB) has been ascribed to the fact that the surface which develops in this sample creates a crystallographic notching which is "effective" in reducing the life. This is not to say that notches do not develop in the other samples. Rather it means that specimen 15 behaves differently than the other samples because (1) the strain level is low so that damage is localized and notches are not blunted by the extensive



plastic flow, (2) crystallographic notches are tending to become the dominant surface feature at lower strains, and (3) the softer material develops more extensive localized plasticity in fewer cycles, much earlier in the life based on the bulk resistance. As suggested earlier in regard to Figure 14(d), this tendency (exhibited here at  $\Delta\epsilon_3$  for HTB and expected for HTA and AR at still longer lives and lower strains) would lead to the so called rocking chair effect evident in Figure 15. But further study is needed before this can be discussed in other than a speculative fashion.

#### Damage Assessment and Accumulation Predictions for Block Cycling

To this point, the discussion of the history dependence of fatigue resistance has focussed on IPS and IOS histories followed by CA cycling. One interesting implication of the application of the postulate to these results is that the current hysteresis loop shape and deformation resistance dictates which fatigue resistance curve should be used to assess damage per cycle. Differences in deformation resistance are due to transient hardening or softening, or in general mean stress relaxation and cyclic creep as well. They may also be due to hardening in tensile or compressive excursions along the skeleton (monotonic) deformation curve.

The postulate suggests that nonlinearities in damage analysis for block cycling arise due to transients taking place within the blocks, and to differences in the resistance curves associated with the stable deformation response that may develop if a block is sufficiently long. For example, consider a history composed of two constant amplitude blocks, with each of these blocks being repeated alternately until initiation. For tests in which all transients occur in the first pair of blocks, the postulate suggests that a range of resistance curves are needed during the first pair, and thereafter a single pair of resistance curves are sufficient for all subsequent blocks. In situations where transient action persists for several blocks, nonlinearities continue over those blocks. In this case the postulate requires assessment of damage using distinctly different resistance curves depending on the transient behavior in each block. Ultimately, if the transients washout, different resistance curves (one for each block) define the materials fatigue

resistance until initiation. In this respect, block cycling provides an interesting test of the viability of the postulate. For this reason tests have been done using low-high (lo-hi) strain and hi-lo strain block cycling. Test conditions are detailed in Table 1 while the results are presented in Tables 5 and 6.

Analysis of the block cycling results would in general require presenting the fatigue resistance trends presented in Figures 14 and 17 as a function of the material's deformation response. For the sake of convenience in analysis, these resistance curves should be expressed as continuous functions normalized with respect to one of the material conditions. This would permit simple yet convenient interpolation over the range of deformation behaviors observed. Furthermore the analysis would best be done numerically, assessing damage per cycle and intergrating this subject to the failure criterion that a sum of unity defines initiation in the spirit of Figure 2. Such a numerical formulation is desirable, but is not warranted for this preliminary investigation involving two rather simple tests. For this reason, bounding resistance curves have been used to simplify this preliminary analysis, and a variant of the dissipated energy formulation--the product  $s_{mx}\Delta e^t$ --is used as a damage paramter. The results therefore, are approximate compared to what could be achieved with a more detailed numerical formulation.

Consider first the results for the lo-hi history--specimen 23. The first  $10^4$  cycles of this test are identical to that for specimen 15 (HTB material). For this reason the correct initial resistance curve is that for HTB material, results for which are plotted in Figure 18. At  $\Delta e_3 = 0.00337$  and  $s_{mx} = \Delta s/2 = 180.65$  MPa for the block, the damage level/cycle  $D = s_{mx}\Delta e^t = 0.606$  MPa so that the expected life is 34,000 cycles. Therefore, the damage/block  $D_B = 0.294$  and, the residual damage capacity,  $D_r = 1 - \sum D_B = 0.706$ . This history does little to harden the HTB and so the HTB resistance curve also reasonably represents the resistance at the end of the first block. The second block of cycles is the high block, which involves 10 cycles identical to the IOS. Based on results for the HTB material subjected to 20 cycles of this IPS (specimen 18) it is expected that the material hardens and then softens during this block. Such hardening and softening is observed, the stress response approaching 321.1 MPa, indicating according to the postulate

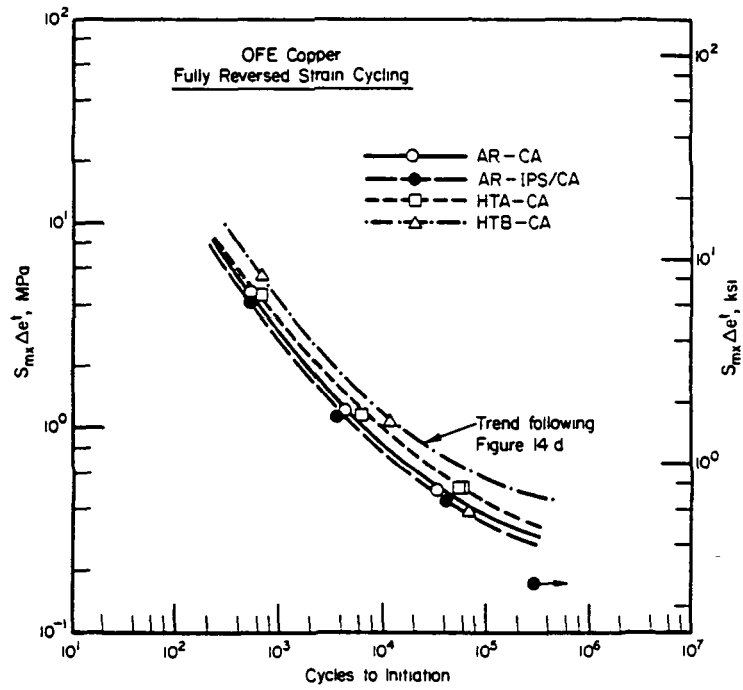


FIGURE 18. FATIGUE RESISTANCE AS A FUNCTION OF  $s_{mx} \Delta \epsilon^t$

that a resistance curve comparable to that for AR material is appropriate. Using  $\Delta e^t = 0.0204$  and  $s_{mx} = 452/2$  MPa,  $D = 4.61$  MPa so that  $N_i = 490$  cycles, and  $D_B = 0.0204$  which leaves  $D_r = 0.706 - 0.0204 = 0.686$ .

The next and all subsequent lo blocks show that the material softens quickly to a nearly stable stress range  $\Delta s = 283.86$  MPa. At  $\Delta e_3 = 0.00337$ ,  $D = 0.47$  MPa. The resistance curve for this case corresponds to HTB material softened by an IOS to  $\Delta s = 280$  MPa cycling at  $\Delta e = 0.00337$ . Examination of the deformation responses for the various material conditions listed in Table 5 indicates that a resistance curve between HTA and HTB, but closer to HTA would be associated with the observed combination of stable stress and strain. Using the lower bound curve (the HTA resistance curve), this value of  $D = 0.47$  MPa corresponds to a life of about 74,000 cycle so that  $D_B = 0.1351$ . The next and all subsequent hi blocks are reasonably represented by a stress range  $\Delta s = 463$  MPa at  $\Delta e = 0.0204$ , so that  $D = 4.72$  MPa. Examining the deformation responses listed in Table 5 indicates this behavior is also bounded by the HTB and HTA conditions, and again the HTA (lower bound) most closely corresponds to the observed behavior. AT  $D = 4.72$  MPa, the life expected based on HTA is 602 cycles, so that the damage per lo-hi pair,  $D_{LH} = 0.0166 + 0.1351 = 0.1517$  for each pair of blocks. Thus the number of blocks remaining is 4.52, or 45,252 cycles. This number of cycles, when added to the earlier analyzed pair of 10,010 cycles, indicates a predicted life of 55,262 cycles.

The predicted life is essentially identical to the observed life of 55,084 cycles to initiation. It should be noted, because of the preliminary nature of the study, that approximations were made to simplify the calculations. But in performing these calculations an attempt has been made to make offsetting simplifications. For this reason, transients have been ignored, which tends to reduce damage somewhat, whereas lower bound resistance curves have been used which tends to overestimate damage. While these approximations offset, the exact extent of this approximation and the related error will remain uncertain until the damage algorithm has been coded for numerical evaluation. Bear in mind that these same approximations carry over into the analysis of the hi-lo BC history which follows.

Specimen 22 has been subjected to the hi-lo history detailed in Table 1, results for which are reported in Table 5. Study of the stable

stress response for the high blocks indicates the hardening during the first block is similar to that for the AR condition. The second block stabilizes at stresses similar to that for the HTA condition, whereas in subsequent blocks the deformation response is comparable to the HTB condition. Corresponding results for the low blocks indicate the deformation response in the first block is like that of the HTA condition, while that of the second and third blocks lies between the HTA and HTB conditions (but is close to the HTA lower bound). Subsequent low blocks soften to a state for which the lower bound is reasonably represented by a trend midway between the HTA and HTB conditions.

Analysis of the first 10 cycles indicates  $D = 0.0204 \times 526/2$  MPa = 5.37 MPa, for which  $N_i = 375$  cycles and  $D_B = 0.0267$ . The next  $10^4$  cycles occur at  $D = 0.501$  for which  $N_i = 60,000$  and  $D_B = 0.1667$  leaving  $D_r = 0.807$  after the first hi-lo pair. The next pair does less damage, the values being  $D = 4.63$  MPa and  $D = 0.478$  MPa for the hi and lo blocks, respectively. Corresponding lives to initiation are respectively 535 and 75,000 cycles, which yields  $D_B = 0.0187$  and  $D_B = 0.133$  for a sum,  $D_{LH}$ , of 0.152 leaving  $D_r = 0.655$ . The third pair of hi-lo blocks involves  $D = 4.63$  MPa and  $D = 0.478$  respectively. Corresponding lives to initiation are 700 cycles and 75,000 cycles, which yields  $D_B = 0.0143$  and  $D_B = 0.133$  for a sum,  $D_{LH}$ , of 0.148 leaving  $D_r = 0.5074$ . The fourth and all subsequent blocks are similar in terms of damage per cycle. All high blocks share the HTB resistance curve while all low blocks share a resistance curve between HTA and HTB. The values of  $D = 4.47$  MPa and  $D = 0.468$  MPa are associated with lives to initiation of 740 cycles and 77,500. (The last result is based on HTA, a lower bound life which overestimates damage.) Damage per block,  $D_B = 0.0135$  and  $D_B = 0.129$ , yields a sum  $D_{LH} = 0.1425$ , so that the remaining number of blocks to failure is  $0.5074/0.1425 = 3.56$ , or 35,631 cycles. The predicted total life thus is  $35,631 + 30,030 = 65,661$  cycles, as compared to an observed life of 73,260 cycles.

While the prediction for the hi-lo case does not match that observed as closely as did the lo-hi case, the result does match the qualitative trend to much longer life. Indeed, if, (as the deformation response suggests) a resistance curve biased away from the HTA toward the HTB condition is used, much of the discrepancy between predicted and observed lives disappears.

Results of the reanalysis indicates a predicted life between 70,000 to 85,000 cycles, depending on where the resistance curve is placed between the HTA lower bound and the HTB upper bound.

### Commentary

Damage analysis of the BC results as well as the IPS and IOS histories using history dependent resistance curves consistent with the postulate correctly predicts trends observed in all cases, including the lo-hi and hi-lo tests. On the other hand the usual strain based linear analysis fails to account for the IPS/IOS trends, and predicts the same life for both BC histories--about 60,919 cycles.

The successes with the IPS/IOS results aside, one could still argue that the above differences in observed lives for lo-hi and hi-lo BC histories develop as a result of scatter, so that successful prediction of any observed life is fortuitous. While such an argument cannot be proven incorrect, the trends for BC histories in the literature, coupled with the nearly 20,000 cycles difference in lives observed herein suggest this argument is vacuous. It could also be argued that statistical scatter in subsequent similar tests would cover a sufficiently broad range of lives such that predictions close to any of the one shot test results reported herein are in general of little consequence. Again such an argument is difficult to prove wrong. But, one must bear in mind that the framework advance herein does not predict a fixed life for a given strain controlled test history. That is, different lives are predicted by this damage postulate to the extent that differences in deformation response develop. For this reason arguments related to scatter are equally vacuous in the present context.

While the postulate advanced holds promise, it has only been applied in situations for which differences in surface topography were a minor factor. This was not by design, as evident in attempts to experimentally develop surface effects by tests such as 100 IOS cycles at  $\Delta e = 0.02$  followed by  $\Delta e_3$  to failure. For this reason, it remains to explore the viability of the postulate at longer lives (lower strains) where surface will be a factor. It likewise remains to examine the postulate in engineering alloys, as well as in combination with other damage mechanisms.

It should be noted in closing that the postulate advanced is rather general. For example, in the absence of surface effects one has:

$$\underline{s} = \underline{s}(e) \quad (4)$$

which defines the current (history dependent) deformation state, and it is postulated that damage per cycle,  $\underline{D}$ , and the damage resistance,  $\underline{R}$ , are also history dependent

$$\begin{aligned} \underline{D} &= \underline{D}(\underline{s}, e, \dots) \text{ , and ,} \\ \underline{R} &= \underline{R}(\underline{s}, e, \dots) \text{ .} \end{aligned} \quad (5)$$

Equations of the form of Eq. (5) have been shown by the data developed herein to hold for a variety of conditions. In general the resistance will also have to be related to the surface topography,  $S$ , and residual stress state,  $\underline{g}$ , which may be step functions of  $\underline{R}$ , once a threshold is reached. That is, more generally,

$$\underline{R} = \underline{R}_1(\underline{s}, e, \underline{e}^P, S, \underline{g}, \dots) \quad (5a)$$

By analogy to the results and postulate for fatigue damage, a similar more general postulate and, similar equations could be written for creep fatigue, or thermal-mechanical fatigue, but care must be taken to include the appropriate rate dependence in Eq (4) and differences in surface effects (wedging, area loss, etc.) in Eqs. (5) and (5a). Simple equations of the form of Eqs. (4) and (5) have already been proposed (e.g., see [12]), and shown to be useful on a limited basis.

#### SUMMARY

The objective of this program was to assess the viability of a damage postulate which asserted that the fatigue resistance curve of a metal is history dependent due to inelastic action. The study focussed on OFE copper because this simple model material accentuated the inelastic action central to

the damage postulate. Given the novel nature of the postulate, the scope of the study was limited to that of a preliminary evaluation. The study carried out was purely phenomenological. Data relevant to damage evolution and crack initiation were developed via a study of surface topography. The effect of surface layer residual stresses were explored via comparative testing as were the effects in initial prestraining.

The results of the study very clearly indicated the deformation history dependence of the fatigue resistance of OFE copper. Furthermore the concept of deformation history dependence was shown to qualitatively explain the fatigue resistance of all histories considered. Likewise quantitative predictions for block cycle histories were found to accurately track the observed results. In this respect the assertion that damage per cycle for a given level of the damage parameter is deformation history dependent appears to be physically justified. Also, use of a history dependent nonlinear assessment procedure consistent with the postulate provided qualitative and accurate quantitative predictions of life to form a small crack when damage was linearly accumulated. For this reason the nonarbitrary linear accumulation assumption appears to be valid when nonlinearities in assessment were accounted for. Double linear accumulation criteria [42,43] which deal separately with initiation and propagation would properly deal with initiation provided some nonlinear assessment scheme were adopted.

### CONCLUSIONS

Many conclusions can be drawn as a result of this study. Among the more significant are the following.

- The use of simple damage parameters such as strain range may lead to errors in adapting constant amplitude data to damage analysis of variable amplitude histories.
- Transients driven by cyclic inelastic action may violate the linear damage accumulation assumption in the reference constant amplitude data base. This coupled with the use of simple damage parameters may effectively preclude adapting constant amplitude data for damage analysis of complex histories in terms of this linear assumption.



- The fatigue resistance curve of a material is deformation history dependent.
- When a deformation history dependent resistance curve is used in damage analysis, accurate qualitative and quantitative predictions for variable amplitude histories can be made in terms of a linear accumulation criterion, up to the initiation of a small crack.

REFERENCES

1. Matsuishi, M., and Endo, T., "Fatigue of Metals Subjected to Varying Stress", Paper presented to Japan Society of Mechanical Engineers, Fukouka, Japan, March 1968; see also Endo, T., Mitsunaga, K., Takahashi, K., Kobayashi, K., and Matsuishi, M., "Damage Evaluation of Metals for Random or Varying Load", Paper presented at 1974 Symposium on Mechanical Behavior of Materials, Kyoto, August, 1974.
2. Dowling, N. E., "Fatigue Life and Inelastic Strain Response Under Complex Histories for an Alloy Steel", J. of Testing and Evaluation, Vol. 1, (4), July, 1973.
3. Wetzel, R. M., "A Method of Fatigue Damage Analysis", Ph.D. Thesis, University of Waterloo, 1971.
4. Jhansale, H. R., "Inelastic Deformation and Fatigue Response of Spectrum Loaded Axial and Flexural Members", Ph.D. Thesis, University of Waterloo, March, 1971.
5. Conle, F. A., "A Computer Simulation Assisted Statistical Approach to the Problem of Random Fatigue", M.A.Sc. Thesis, University of Waterloo, March, 1974.
6. Landgraf, R. W., Richards, F. D., and LaPointe, N. R., "Fatigue Life Predictions for a Notched Member Under Complex Loading Histories", SAE AE-6, SAE, 1977, pp 95-106.
7. Leis, B. N., "Fatigue Analysis to Assess Crack Initiation Life for Notched Coupons and Complex Components", Ph.D. Thesis, University of Waterloo, September, 1976.
8. Morrow, J. D., in Fatigue Design Handbook, SAE, Chapter 3.2, 1968.
9. Smith, K. N., Watson, P., and Topper, T. H., "A Stress-Strain Function for the Fatigue of Metals", SMD Report 21, University of Waterloo, October, 1969; see also, Smith, K. N., Watson, P., and Topper, T. H., "A Stress-Strain Function for the Fatigue of Metals", J. of Matls., JMLSA, Vol. 5 (4), pp 767-778, December, 1970.
10. Haibach, E., and Lehrke, H. P., Das Verfahren der Amplituden-Transformation, LBF Report No. FB-125, LBF Darmstadt, 1975.
11. Ostergren, W. J., "A Damage Function and Associated Failure Equations for Predicting Hold Time and Frequency Effects in Elevated Temperature Low Cycle Fatigue", J. Testing and Evaluation, Vol. 4, No. 5, pp 327-339, 1976.

12. Leis, B. N., "An Energy-Based Fatigue and Creep-Fatigue Damage Parameter", Journal of Pressure Vessel Technology, Trans. ASME, Vol. 99, No. 4, pp 524-533, November, 1977.
13. Leve, H. L., "Cumulative Damage Theories", in Metal Fatigue: Theory and Design, Wiley, 1969.
14. Schijve, J. "Estimation of Fatigue Performance of Aircraft Structures", in Fatigue Testing of Aircraft Structures, ASTM STP 338, 1961, pp 193-201.
15. Libertiny, G. Z., Topper, T. H., and Leis, B. N., "The Effect of Large Pre-Strains on Fatigue", Experimental Mechanics, Vol. 17, No. 2, pp 64-68, February, 1977.
16. Leis, B. N., and Laflen, J. H., "An Energy Based Postulate for Damage Assessment of Cyclic Nonproportional Loadings with Fixed Principal Directions", Proceedings ASME Symposium on Ductility and Toughness in Elevated Temperature Service, San Francisco, MPC-8, pp 371-389, November, 1978.
17. Leis, B. N., and Forte, T. P., "Fatigue Damage Analysis Under Variable Amplitude Cycling", in Random Fatigue Life Prediction, ASME, to appear, 1983.
18. Morrow, J. D., Wetzel, R. M., and Topper, T. H., "Laboratory Simulation of Structural Fatigue Behavior", Effects of Environment and Complex Load History on Fatigue Life, ASTM STP 462, pp 74-91, 1970.
19. Leis, B. N., Gowda, C.V.B., and Topper, T. H., "Cyclic Inelastic Deformation and the Fatigue Notch Factor", Cyclic Stress-Strain Behavior Analysis, Experimentation and Failure Prediction, ASTM STP 519, American Society for Testing and Materials, pp 133-150, 1973.
20. Morrow, J., "Cyclic Plastic Strain Energy and Fatigue of Metals", Internal Friction, Damping, and Cyclic Plasticity, ASTM STP 378, American Society for Testing and Materials, 1965, pp 45-84.
21. Basquin, O. H., "The Exponential Law of Endurance Tests", Proc. ASTM, Vol. 10, pp 625-630, 1910.
22. Coffin, L. F., "A Study of Cyclic Thermal Stresses in a Ductile Metal", Trans. ASME, Vol. 76, pp 931-950, 1954.
23. Manson, S. S., "Behavior of Materials Under Conditions of Thermal Stress; Heat Transfer", Proc. Symposium, U. of Michigan Engr. Research Inst., pp 9-75, 1953.
24. Broek, D., and Leis, B. N., "Similitude and Anamolies in Crack Growth Rates", in Materials, Experimentation, and Design in Fatigue, Westbury House, IPC Science Press, UK, pp 129-146, March, 1981.

25. Leis, B. N., "Predicting Crack Initiation Fatigue Life in Structural Components", in Methods of Predicting Fatigue Life, ASME, pp 57-76, 1979.
26. Palmgren, A., "Die Lebensdauer von Kugellagern", VDI-Z, Vol. 69, pp 337-341, 1929.
27. Miner, M. A., "Cumulative Damage in Fatigue", J. of App. Mech., Vol. 12, pp A-159, 1945.
28. Landgraf, R. W., "The Resistance of Metals to Cyclic Deformation", in Achievement of High Fatigue Resistance in Metals and Alloys, ASTM STP 467, 1970, pp 3-36.
29. Jhansale, H. R., "Inelastic Deformation and Fatigue Response of Spectrum Loaded Axial and Flexural Members", Ph.D. Thesis, University of Waterloo, March, 1971.
30. Forsyth, P.J.E., "The Physical Basis of Metal Fatigue", Blackie and Son Ltd., London, 1969.
31. Allery, M.B.P. and Birkbeck, G., "Effect of Notch Root Radius on the Initiation and Propagation of Fatigue Cracks", Engr. Fract. Mech., Vol. 4, No. 2, June 1972, pp. 325-331.
32. Pangborn, R. N., Weissmann, S., and Kramer, I. R., "Dislocation Distribution and Prediction of Fatigue Damage", Metallurgical Transactions A, Vo. 12A, 1981, pp 109-119.
33. Mughrabi, H., Ackermann, F., and Herz, K., "Persistent Slip Bands in Fatigued Face Centered and Body Centered Cubic Metals", Fatigue Mechanisms, ASTM STP 675, pp 69-105, 1979.
34. Laird, C., "Recent Advances in Understanding the Cyclic Deformation of Metals and Solid Solutions", in Work Hardening in Tension and Fatigue, AIME, pp 150-176, 1976.
35. Kocanda, K., Fatigue Failure of Metals, Noordhoff, 1978.
36. Brick, R. M., Gorden, R. E., and Phillips, A., "Structure and Properties of Alloys", McGraw-Hill, Third Edition.
37. Katagiri, K., Omura, A., Koyanagi, K., Awatani, J., Shiraishi, T., and Kaneshiro, H., "Early Stage Crack Tip Dislocation Morphology in Fatigued Copper", Metallurgical Transactions A, Vol. 8A, 1977, pp 1769-1773; see also, Katagiri, K., Awatani, J., Omura, A., Koyanagi, K., and Shiraishi, T., "Dislocation Structures Around the Crack Tips in Early Stage in Fatigue of Iron", Fatigue Mechanisms, ASTM STP 675, 1979, pp. 106-128.
38. Pratt, J. E., "Dislocation Subfracture in Strain-Cycled Copper, Journal of Materials, Vol. 1, No. 1, March, 1966, pp. 77-88.

39. Watson, P., "The Effect of Mean Stress and Overstrain on the Fatigue Behavior of Structural Steels", Ph.D. Thesis, University of Waterloo, 1971.
40. Gowda, C.V.B., Leis, B. N., and Smith, K. N., "Dependence of Notch Strength Reduction Factor on Plasticity and Duration of Crack Growth", Journal of Testing and Evaluation, ASTM, Vol. 2, No. 1, pp 57-61, January, 1974.
41. Landgraf, R. W., and La Pointe, N. R., "Cyclic Stres-Strain Concepts Applied to Component Fatigue Life Prediction", SAE Transactios, Vol. 83, Sect. 2, 1974, pp. 1198-1207.
42. Grover, H. J., "An Observation Concerning the Cycle Ratio in Cumulative Damage", Fatigue in Aircraft Structures, ASTM STP 274, 1960, pp. 120-124.
43. Manson, S. S., Freche, J. C., and Ensign, C. R., "Application of a Double Linear Damage Rule to Cumulative Fatigue", Fatigue Crack Propagation, ASTM STP 415, 1967, pp. 384.